Applied Catalysis B: Environmental 89 (2009) 167–182

Contents lists available at ScienceDirect

Applied Catalysis B: Environmental

journal homepage: www.elsevier.com/locate/apcatb

Hydrocarbon production via Fischer–Tropsch synthesis from H_2-poor syngas over different Fe-Co/γ-Al_2O_3 bimetallic catalysts

Sara Lögdberg [a], Dewi Tristantini [b], Øyvind Borg [c,1], Lars Ilver [d], Börje Gevert [b,*], Sven Järås [a], Edd A. Blekkan [c], Anders Holmen [c]

[a] Royal Institute of Technology (KTH), Chemical Technology, S-100 44 Stockholm, Sweden
[b] Chalmers University of Technology, Department of Chemical and Biological Engineering, S-412 96 Gothenburg, Sweden
[c] Norwegian University of Science and Technology (NTNU), Department of Chemical Engineering, N-7491 Trondheim, Norway
[d] Chalmers University of Technology, Department of Applied Physics, S-412 96 Gothenburg, Sweden

ARTICLE INFO

Article history:
Received 15 May 2008
Received in revised form 27 November 2008
Accepted 30 November 2008
Available online 6 December 2008

Keywords:
Fischer–Tropsch synthesis
H_2-poor synthesis gas
Low H_2/CO ratio
Water–gas-shift
Cobalt
Iron
Bimetallic catalysts
Alloy

ABSTRACT

Fischer–Tropsch synthesis (FTS) at 20 bar and 483 K, with H_2-poor syngas (H_2/CO ratio = 1.0) in order to simulate gasified biomass, was performed over Al_2O_3-supported catalysts with various ratios of Fe:Co (12 wt% bimetal) prepared by co-impregnation. Co was found to be incorporated into the Fe_2O_3 phase after calcination, at least for the iron-rich samples, while no evidence of Fe incorporated into Co_3O_4 was found. Upon reduction, most probably FeCo alloys were formed in the iron-rich bimetallic samples. The degree of reduction of the catalysts showed a non-linear behavior with respect to the Fe:Co ratio, but it is obvious that Co increases the reducibility of Fe. Alloying Co with small/moderate amounts of Fe improved the FT activity compared to the 100% Co catalyst at low conversion levels. Alloying Fe with small/moderate amounts of Co lowered the FT activity, but increased the relative water–gas-shift (WGS) activity compared to the 100% Fe catalyst. However, the overall WGS activity was very low for all catalysts, even with external water addition to the feed, resulting in low FT productivities (per gram catalyst) due to the low partial pressure of H_2. A higher Fe:Co ratio in the bimetallic catalyst generally resulted in higher relative WGS activity, but did not lower the H_2/CO usage ratio to the desired value of 1.0. For the Fe-containing catalysts, the space–time yield of hydrocarbons (HCs) decreased with increasing partial pressure of water or reduced space velocity, indicating an inhibition of water on the FT activity, most often resulting in low FT productivity under the conditions with highest relative WGS activity (usage ratios closest to the inlet H_2/CO ratio). Moreover, the co-impregnation technique resulted in a surface enrichment of Fe, at least for the Co-rich samples, covering the Co sites. For the bimetallic catalysts, both FT and WGS activities rapidly declined at high partial pressure of water due to deactivation by oxidation and sintering. However, the results indicate that WGS and FT proceeded over sites of different nature in the bimetallic catalysts.

The bimetallic catalysts showed essentially no synergy effects with respect to HC selectivities and olefin/paraffin ratios, which partly can be explained by the use of a sub-stoichiometric H_2/CO ratio as feed. The higher the Fe content, the lower were the C_{5+} selectivity and C_3 olefin/paraffin ratio. Water addition increased the C_{5+} selectivity and C_3 olefin/paraffin ratio and reduced the CH_4 selectivity.

1. Introduction

Syngas obtained from gasification of biomass or coal typically has a lower ratio of hydrogen to carbon monoxide (H_2/CO) compared with syngas produced from natural gas [1–3]. Direct utilization of this H_2-poor syngas inside a Fischer–Tropsch synthesis (FTS) reactor with its potential advantages is possible only if the water–gas-shift (WGS) reaction occurs simultaneously, providing a high enough molar H_2/CO ratio throughout the reactor. The water needed in the WGS reaction (1.2) is produced in the FT reaction (1.1), but may also be added externally.

$$\text{FTS}: \quad CO + 2H_2 \rightarrow -CH_2- + H_2O \tag{1.1}$$

$$\text{WGS}: \quad CO + H_2O \leftrightarrow CO_2 + H_2 \tag{1.2}$$

For a process to be able to reach 100% syngas conversion (theoretically), the inlet H_2/CO ratio must equal the H_2/CO usage ratio, which also implies that the average H_2/CO ratio throughout

* Corresponding author. Tel.: +46 31 7722956; fax: +46 31 160062.
E-mail address: gevert@chalmers.se (B. Gevert).
[1] Current address: StatoilHydro Research Center, postuttak N-7005, Trondheim, Norway.

0926-3373/$ – see front matter.
doi:10.1016/j.apcatb.2008.11.037

the reactor will be equal to the inlet value. The usage ratio is calculated according to the following equation:

$$\text{Usage ratio of } (H_2/CO) = \frac{3xS_{CH_4} + FxS_{C_2-C_4} + 2xS_{C_{5+}} - S_{CO_2}}{100}$$

where S indicates total carbon atom selectivity. The factors multiplied with each selectivity indicate the number of H_2-moles required for one CO-mole to form the product. The above equation only applies if the CO_2 is formed in the WGS reaction (1.2). The usage ratio may also be calculated from the CO and H_2 conversions and the inlet H_2/CO ratio.

For a FT catalyst with no WGS activity, the usage ratio is approximately 2.1, i.e. equal to the stoichiometric value required by reaction 1.1. Feeding such a catalyst, typically cobalt-based, with a H_2-poor syngas (i.e. H_2/CO inlet molar ratio below 2.1) would lead to an even lower H_2/CO ratio at the outlet of the reactor, and to a low maximum possible syngas conversion. However, for a catalytic system possessing WGS activity, it should be possible to achieve a higher conversion of such a H_2-poor syngas into hydrocarbons. In other words, such a catalytic system would possess a low H_2/CO usage ratio. The lowest industrial FTS molar feed H_2/CO ratio is 1.7, which is used in Sasol's coal-based low-temperature Fischer–Tropsch (LTFT) process. The catalyst consists of precipitated and extruded iron promoted with alkali [3,4]. The WGS activity of the iron catalyst makes sure that the H_2/CO ratio inside of the reactor is high enough to satisfy the stoichiometry of reaction 1.1. Since the reaction order of the partial pressure of H_2 has been reported to be positive and of similar magnitude (0.5–1) for both Fe- and Co-based catalysts, there is also a kinetic reason for increasing the H_2/CO ratio of a H_2-poor syngas [5–8].

A supported cobalt-iron bimetallic catalyst seems to be a viable option for the direct conversion of a low H_2/CO ratio syngas into hydrocarbons. Cobalt has a high activity and selectivity to long-chain paraffins but low WGS activity, whereas iron is known to be active for the WGS reaction but its kinetic FT rate is commonly believed to be negatively affected by the partial pressure of water [3,9,10]. Several studies have reported the use of Fe-Co catalysts for FTS with inlet molar H_2/CO ratios above or equal to 2 [11–17]. Mixing the two FT-active metals did not simply give the additive properties of the individual metals [11]. For CO_2-free syngas, the metallic FeCo alloy of the reduced catalysts is believed to be the FT-active phase [18]. The purpose of the present work is to study the combined WGS and FT activity over different Fe:Co ratio catalysts and their selectivity to hydrocarbon products, using syngas with a molar H_2/CO ratio of 1.0. Such a ratio is typical when the syngas is produced from biomass.

2. Experimental

2.1. Catalyst preparation

The incipient wetness co-impregnation method was employed to prepare γ-Al_2O_3 supported catalysts containing total 12 wt% of cobalt and iron. The support used was Puralox SCCa-5/200 from Sasol. Different proportions of aqueous solutions of $Co(NO_3)_2{\cdot}6H_2O$ and $Fe(NO_3)_3{\cdot}9H_2O$, in which cobalt was progressively replaced by iron, were pre-mixed and the resulting solution was heated to 343 K in all cases in which iron was present. The impregnated alumina was dried in air at 383 K for 3 h and then calcined in flowing air at 573 K (ramp: 2 K/min) for 16 h. Catalysts with the following Fe:Co weight ratios were prepared: (a) 0:100 (0 wt% Fe: 12 wt% Co), (b) 5:95 (0.6 wt% Fe: 11.4 wt% Co), (c) 15:85 (1.8 wt% Fe: 10.2 wt% Co), (d) 25:75 (3 wt% Fe: 9 wt% Co), (e) 50:50 (6 wt% Fe: 6 wt% Co), (f) 75:25 (9 wt% Fe: 3 wt% Co) and (g) 100:0 (12 wt% Fe: 0 wt% Co).

2.2. BET surface area

BET surface area measurements were performed on the calcined samples in a TriStar Micromeritics 3000 instrument. The samples were evacuated and dried at 523 K prior to analysis.

2.3. CO chemisorption

Measurements of CO chemisorption were conducted in a standard volumetric glass apparatus (Micromeritics ASAP 2010) after reduction of catalyst in flowing hydrogen at 1 bar, 623 K (ramp: 1 K/min) for 10 h followed by evacuation at 603 K for 1 h and 30 min evacuation at 373 K. A first CO adsorption isotherm was recorded at 313 K in the pressure interval 10–300 Torr. A second adsorption isotherm was subsequently recorded after pumping the sample for 1 h to distinguish weakly adsorbed CO from strongly adsorbed CO. The amount of chemisorbed CO was determined by taking the difference in volume adsorbed between the two isotherms, extrapolating the linear portions of the adsorption isotherms to zero pressure. This was done because it is known that physical adsorption of CO often accompanies the chemisorption [19].

2.4. Temperature-programmed reduction (TPR) and pulse oxidation (PO)

The TPR and the PO experiments have been described elsewhere [20]. Briefly, for the TPR, approximately 0.2 g of catalyst was put in a quartz reactor. The temperature was raised from ambient to 1203 K (ramp: 10 K/min) in 7% H_2 in Ar (30 ml/min) and then held constant at 1203 K for at least 1 h, while monitoring the H_2 uptake by a thermal conductivity detector (TCD). The TPR was performed for the calcined catalysts, for the catalysts (partly) reduced at 503 K for 90 min (see Section 2.5), and for the partly reduced catalysts after being re-oxidized in air at 573 K for 5 h. Calibration of the H_2 uptake was done by reduction of Ag_2O powder.

For the PO experiments, the catalyst samples were first reduced in hydrogen for 16 h at 623 K (ramp: 1 K/min), and then flushed with He for 1 h. Oxygen titration was performed at 673 K. The PO data were used to estimate the degree of reduction of the catalysts, which was calculated assuming the uptake of O_2 to be distributed between the Fe and Co according to the Fe:Co molar ratios in each catalyst. Total oxidation to Fe_2O_3 and Co_3O_4 was assumed [11].

2.5. Mass spectrometer (MS) analysis of products formed during TPR

It is known that with a relatively narrow-pore support such as γ-Al_2O_3, part of the metal nitrates used in the catalysts preparation is stabilized on the catalyst surface during calcination [21,22]. These residual nitrates are decomposed and reduced during reduction of the catalyst samples, hence affecting the TCD signal during TPR. In order to elucidate which TPR peaks that stem from reductive decomposition of residual nitrates in the calcined samples, and hence not from the reduction of the metal oxides, TPR was performed in a thermo-gravimetric analysis set-up (Netzsch STA 449 C) coupled to a mass spectrometer (Netzsch QMS 403 C). The ion currents of *m/e* 18 and 30 were recorded, indicative of water and NO/NO_2, respectively. The same reductive gas and the same heating rate (10 K/min) as in the standard TPR were used.

2.6. X-ray photoelectron spectroscopy (XPS)

The surface concentrations of Co and Fe of the calcined and reduced catalysts were determined using a Perkin Elmer, PHI

5000C, ESCA System. The calcined powder samples (four) were pressed into pieces of indium foil attached to one sample holder. XPS spectra were first taken of the catalysts in the calcined state, after which the sample holder was introduced into a pre-treatment chamber. The samples were reduced at atmospheric pressure in 4% H_2 in Ar at 623 K (ramp: 2 K/min) for 12 h, and then transferred again to the UHV measurement chamber for analysis in the reduced state.

The X-ray source was monochromated Al Kα focused to a sampling area of approximately 0.8 mm × 0.8 mm. The angle between the X-ray source and electron spectrometer was 90 degrees, and the surface sensitivity approximately five atomic layers. Due to the isolating support material (γ-Al_2O_3), the samples had to be neutralized using a flood electron gun. Nevertheless, some shift in binding energy was observed and therefore the energy scale for all spectra was adjusted so as to position the O 1 s signal, mainly originating from γ-Al_2O_3, at the correct binding energy (i.e. at 532 eV). In (indium) 3p was sometimes observed, with $3p_{1/2}$ overlapping the Fe $2p_{3/2}$ region. Spectra were corrected by subtracting an indium reference spectrum with a weight to completely remove In $3p_{3/2}$. The Al Kα has the disadvantage of giving rise to a Co LMM Auger structure close to the energy of Fe 2p. The Co Auger contribution was estimated from the signal of the pure Co catalyst (0Fe-100Co (a)) and subtracted from the spectra.

In order to study the concentration profile in the Fe-Co particles of the reduced samples, Ar^+ sputtering was performed with a Perkin Elmer differential ion gun. The current density was 5 μA/cm^2 at a beam energy of 3 keV, which accomplished the removal of approximately one atomic layer every 20 s. Sputtering times of 100, 200 and 300 s were used for the four samples. Atomic concentrations of Co and Fe were calculated by using MultiPak Software version 6.0.

2.7. X-ray diffraction (XRD)

X-ray diffraction was performed on the calcined samples using a Siemens D5005 X-ray diffractometer with Cu Kα radiation. A secondary monochromator was used. The diffractograms were compared with Powder Diffraction Files (PDFs) of known crystallite phases. Crystallite thickness of Co_3O_4 and Fe_2O_3 was estimated by using the Scherrer formula [19] for the respective 100% peaks. Assuming spherical crystallites, the diameter of the metal oxide particles may be estimated by correcting the crystallite thickness by a factor 4/3 [19]. For some of the catalysts, X-ray diffraction was also performed on the reduced samples. In that case, the samples were reduced in H_2 at 623 K for 16 h and then passivated. The passivation was performed by letting the temperature in the reactor decrease to room-temperature, after which the reactor was flushed by N_2 5.0 for at least 1 h followed by flushing with 0.5% O_2 in N_2 for another hour. Step size (2θ) and step time in XRD were 0.04° and 13 s, respectively.

2.8. Catalytic reaction

The FTS experiments were carried out in a 0.93 cm i.d. stainless steel fixed-bed reactor, in the same manner as described by Storsæter et al. [20]. Briefly, to achieve a close to isothermal bed temperature profile, approximately 1 g of calcined catalyst (53–90 μm) was diluted with 4 g inert material (SiC, particle size 75–150 μm). The catalysts were reduced *in situ* in hydrogen at atmospheric pressure and at 623 K (ramp: 1 K/min) for 16 h. The inlet molar H_2/CO ratio was 1.0 and the feed contained 3 mol% of N_2 as an internal standard. The reaction temperature and pressure were 483 K and 20 bar. In period 1 (lasting 24 h), the gas hourly space velocity (GHSV) was 12 Ndm^3/g_{cat}.h. In period 2, the GHSV was lowered to 3 Ndm^3/g_{cat}.h and held for another 24 h. Catalysts (a–d) were further tested in periods 3 and 4, where 20% and 33% steam were introduced into the feed, respectively, keeping the total pressure at 20 bar and the (dry) syngas flow at 3 Ndm^3/g_{cat}.h. In period 5, the same conditions as in period 2 were used.

In order to make sure that the CO_2 formed in the experiments was mostly from the WGS reaction and hence that the equation used for calculating the usage ratio is correct, the measured H_2/CO usage ratio (from H_2 and CO conversions) was compared with the calculated one. The maximum difference between the calculated and measured usage ratio was estimated to be 2%, which is small enough to suggest that essentially all CO_2 is formed in the WGS reaction.

3. Results and discussion

3.1. Catalyst characterization

Table 1 shows the BET surface area (calcined samples), CO chemisorption, particle size as measured by XRD (calcined samples) and degree of reduction as measured by PO for the catalysts. The nominal metal loadings have been used for all calculated catalyst properties as they agreed reasonably well with analyzed concentrations (measured by ICP-AES).

3.1.1. CO chemisorption

The CO chemisorption results show a dramatic decrease of CO adsorbed as the Fe loading is increased. It is known that when Fe is covering the surface, both the CO uptake and the reducibility decrease, even though the same adsorption stoichiometry of CO on Co and Fe could be assumed [11]. This was the case when Fe was sequentially added to a Co/TiO_2 catalyst [11]. Supported Fe_2O_3 requires a higher reduction temperature than Co_3O_4, and a probable reason for the lower CO uptake in the above study [11] could be inefficient reduction of the Fe_2O_3. In the present study the dramatic decrease in CO uptake with increased content of Fe (catalysts a–d) is not reflected in the degree of reduction (Table 1), in the particle size of the metal precursors (i.e. Co_3O_4 and

Table 1
Characterization results for all catalysts.

Catalyst	Nominal loadings [wt% Fe/wt% Co]	BET surface area [m^2/g catalyst]	CO chemisorption (first–second isotherm) [μmol CO/g catalyst]	Particle sizes of Co_3O_4/Fe_2O_3 [nm][a]	Degree of reduction [%][b]
0Fe-100Co (a)	0/12	174	74	17/–	49
5Fe-95Co (b)	0.6/11.4	156	37	18/n.d.	45
15Fe-85Co (c)	1.8/10.2	145	35	23/n.d.	51
25Fe-75Co (d)	3/9	149	13	19/n.m.	37
50Fe-50Co (e)	6/6	153	8	24/20	47
75Fe-25Co (f)	9/3	157	7	n.m./16	33
100Fe-0Co (g)	12/0	162	7	–/30	24
Al_2O_3 support	–	195	–	–	–

[a] As measured by XRD (n.d. = not detectable, n.m. = not measurable).
[b] As measured by PO, the relative uncertainty ($\pm 2\sigma$) is estimated to ±10% based on repeated measurements.

Fe_2O_3 in the calcined samples, Table 1), or in the FT activity (Table 5 and Fig. 8). The reason for the distinct decrease in CO uptake is believed to be due to a failure to measure the number of active sites in the Fe-containing catalysts, rather than indicating that the low-iron content bimetallic catalysts (b–d) should have much higher site activities than the pure Co catalyst. A probable explanation for the low CO uptake is that Fe is oxidized by traces of H_2O or O_2 from the ambient air upon evacuation at high temperatures [23] and that the evacuation time between the two isotherms was too long. Schanke [24] performed the evacuation between the first and second CO adsorption isotherm for Fe/Al_2O_3 catalysts for only two minutes, as longer evacuation times (1–3 h) almost completely removed the initially adsorbed CO. The "failed" CO adsorption results in the present study indicate that Fe is effectively covering the Co sites. A surface enrichment of Fe in supported Fe-Co bimetallic catalysts is in agreement with the findings of Duvenhage and Coville [11]. The catalysts with similar CO adsorption have very different FT activities, and hence the CO adsorption results in the present study are not at all indicative of activity.

Duvenhage and Coville [11,14] reported successfully measured CO adsorption and FT activity values (at a H_2/CO ratio of 2) for their 10 wt% $Fe-Co/TiO_2$ catalyst series without any visible correlation between the two, which could be explained by different site activities (of Fe, Co and FeCo alloys). For instance, iron is known to have a much lower site activity as compared with Co [11]. Furthermore, no trend between CO adsorption and Fe:Co ratio was obtained in those studies [11,14]. The unsuccessful chemisorption measurements in the present study make it impossible to estimate site activities (TOFs) of the studied catalysts.

Bearing in mind that the CO adsorption values in the present study give an indication of the extent of iron coverage of the metal surface, rather than indicating the number of active sites, the similar amounts of adsorbed CO for catalysts 5Fe-95Co (b) and 15Fe-85Co (c) in the present study, as shown in Table 1, supports the theory that surface segregation of iron is enhanced in the presence of Co (i.e. at lower Fe contents) as reported earlier [14,25].

3.1.2. Temperature-programmed reduction (TPR)

3.1.2.1. Comparison of TPR patterns for the bulk metal oxide materials with the corresponding supported catalysts. Fig. 1A shows the comparison of Co_3O_4 with the corresponding supported catalyst 0Fe-100Co (a). The residual nitrate peak for catalyst (a) appears at 565 K, and should not be included in the comparison with the TPR profile of bulk Co_3O_4. The reduction of Co_3O_4 in H_2 takes place in two consecutive steps [22,26]:

$$Co_3O_4 + H_2 \rightarrow 3CoO + H_2O \quad (3.1)$$

$$3CoO + 3H_2 \rightarrow 3Co + 3H_2O \quad (3.2)$$

resulting in a need of 2.67 H/Co for complete reduction. These two steps are clearly visible for both the bulk Co_3O_4 and catalyst (a), the first step comprising about 22% and 29% of the total H_2 uptake for the two samples, respectively. The theoretical value is (1/4), i.e. 25%, and deviations from this value for the bulk Co_3O_4 is due to difficulties in separating the two peaks. As to catalyst (a), the higher value is probably due to incomplete reduction of CoO [22] or due to the formation of hard-to-reduce Co-support species during the TPR [27] that are not completely reduced at 1203 K. It has been reported that Co(II) [27] may enter some of the tetrahedral vacancies of the defect spinel structure of γ-Al_2O_3 upon reduction (i.e. not visible by XRD), without forming a stoichiometric spinel. It is obvious that supporting Co_3O_4 on γ-Al_2O_3 shifts the TPR peaks to higher temperatures, indicating a strong interaction between Co_3O_4 and the support. The broad peak with maximum at about 930 K is due to the reduction of differently sized CoO particles

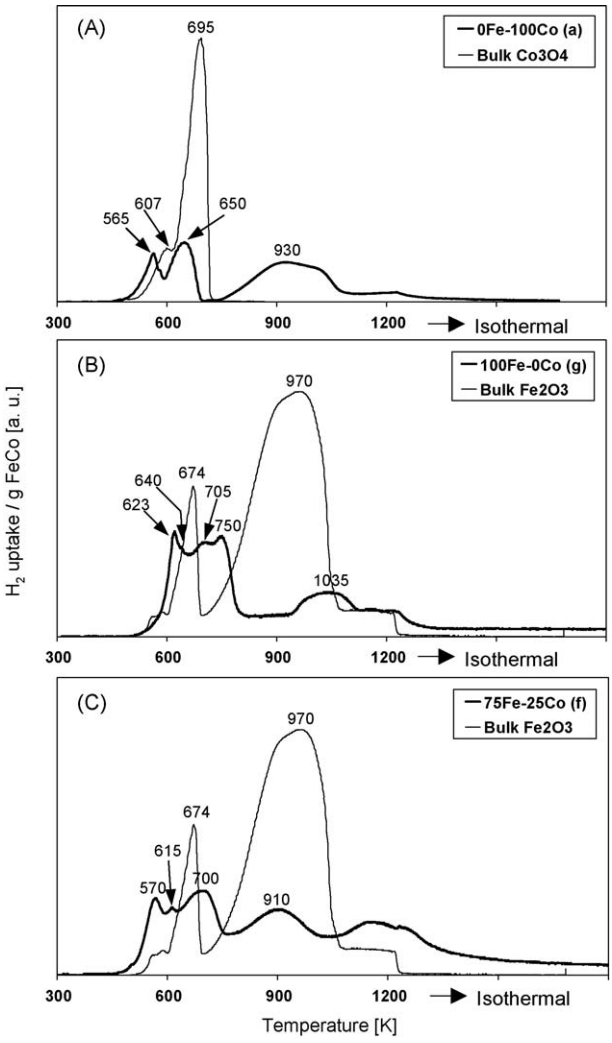

Fig. 1. TPR profiles of A: bulk Co_3O_4 and 0Fe-100Co (a), B: bulk Fe_2O_3 and 100Fe-0Co (g), C: bulk Fe_2O_3 and 75Fe-25Co (f). In frame A, the scale on the *y*-axis reaches a three times higher value than the scales in B and C.

interacting with various strengths with the support material to metallic Co [22,26], smaller particles interacting more strongly with the support and hence being reduced at higher temperatures. The bulk Co_3O_4 has an average crystallite size of 53 nm, while that of catalyst (a) amounted to 17 nm.

Fig. 1B shows the comparison of Fe_2O_3 with the corresponding supported catalyst 100Fe-0Co (g). The residual nitrate peak for catalyst (g) appears at 623 K and should not be included in the comparison with the TPR profile of bulk Fe_2O_3. The reduction of Fe_2O_3 in H_2 takes place in two (reaction 3.3 and the combination of 3.4 and 3.5) or three consecutive steps (3.3, 3.4 and 3.5), depending on the temperature used for reduction and on the temperature ramping rate during TPR [28]:

$$3Fe_2O_3 + H_2 \rightarrow 2Fe_3O_4 + H_2O \quad (3.3)$$

$$2Fe_3O_4 + 2H_2 \rightarrow 6FeO + 2H_2O \quad (3.4)$$

$$6FeO + 6H_2 \rightarrow 6Fe + 6H_2O \quad (3.5)$$

resulting in a need of 3 H/Fe for complete reduction. The FeO was reported to be thermodynamically stable above 843 K and formed during TPR with high ramping rate (5–10 K/min). FeO can also possibly be stabilized on support materials [28]. The two or three reactions are easily identified in the TPR pattern of the bulk Fe_2O_3,

where the first peak comprises 14% of the total H_2 uptake. The theoretical value would be (1/9), i.e. 11%. For catalyst (g), however, the TPR pattern is much more complex, indicating a strong interaction between the Fe_2O_3 and the support, typically seen from the high-temperature peak at 1035 K. The lower total H_2 uptake of this catalyst compared to the bulk Fe_2O_3 indicate the formation of hard-to-reduce Fe-Al spinels (or other Fe-Al species) during the TPR experiment ([29] and references therein) that are not reduced at 1203 K. It is reasonable to assume that these Fe-Al spinels could only form during reduction since they contain Fe(II), which is not present in the precursor $Fe(NO_3)_3{\cdot}9H_2O$. The same would apply for the potential penetration of Fe(II) into the tetrahedral vacancies of the defect spinel structure of γ-Al_2O_3, as mentioned above for Co [27].

The fact that catalyst (g) has a higher total H_2-uptake before 800 K compared to the unsupported bulk Fe_2O_3 is puzzling. A possible explanation for a shift towards lower temperatures of the supported Fe_2O_3 is probably that FeO is stabilized by the support material and therefore is formed at lower temperatures than in the bulk sample, which in turn makes the formation of metallic Fe taking place at lower temperature. The H_2 uptake of the low-temperature peaks (< 800 K) for catalyst (g) is significantly larger than what could theoretically be explained by reaction 3.3, which implies that these peaks also correspond to further reduction of the Fe_3O_4. Possibly, the three low-temperature peaks for catalyst (g) at 640, 705 and 750 K correspond to the three sequential reduction steps of Fe_2O_3 to Fe (i.e. reaction 3.3–3.5), but leaving an essential part of the iron unreduced. The bulk Fe_2O_3 has an average crystallite size of 27 nm, which is essentially the same as for catalyst (g) (30 nm).

3.1.2.2. Interpretation of the TPR patterns of the catalyst samples. The TPR patterns of the calcined catalysts, with the correction for the residual nitrates, are shown in Figs. 2 and 3. The MS analyses showed that all calcined catalyst samples had residual nitrates but in much smaller amounts than the 0Fe-100Co (a) catalyst. The pure iron catalyst (100Fe-0Co (g)) had almost no residual nitrates, which can be explained by iron nitrate decomposing at lower temperatures than cobalt nitrate. When correcting the TPR patterns of calcined samples for the residual nitrates it was

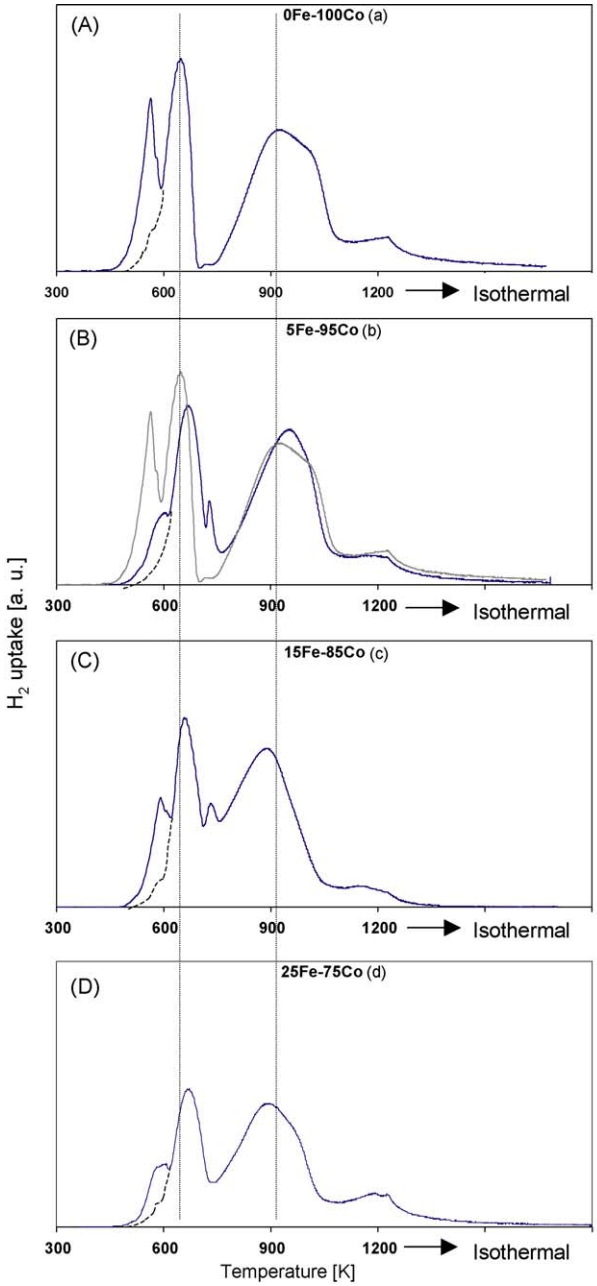

Fig. 2. TPR profiles of the Co-rich catalysts (a–d). Catalyst weight = 0.2 g, temperature ramp = 10 K/min. Dashed lines indicate the positions of the main peaks of catalyst (a). In frame B, TPR profiles of both catalyst (b) and (a) are depicted for comparison.

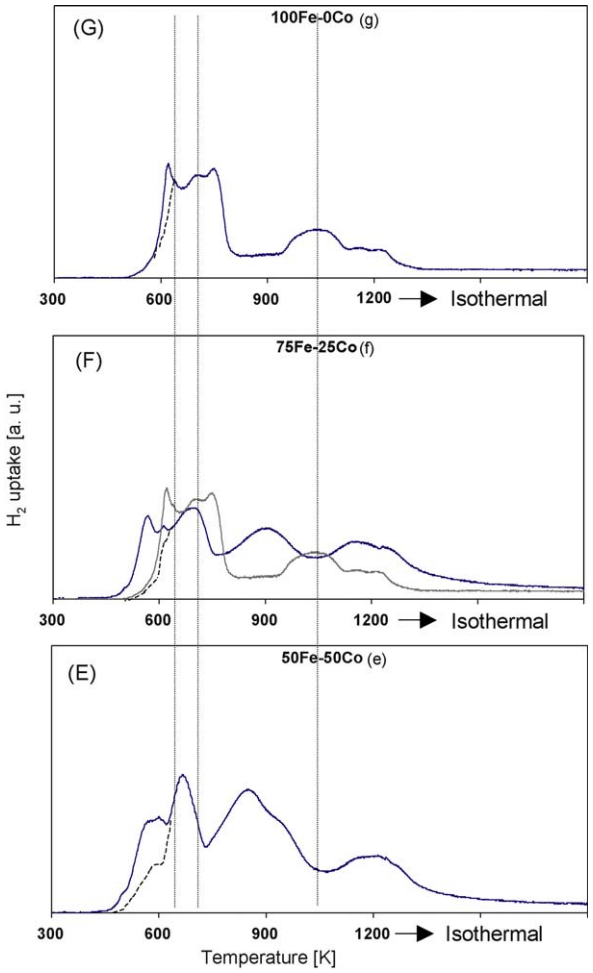

Fig. 3. TPR profiles of the Fe-rich catalysts (g–e). Catalyst weight = 0.2 g, temperature ramp = 10 K/min. Dashed lines indicate the positions of three chosen peaks of catalyst (g). In frame F, TPR profiles of both catalyst (f) and (g) are depicted for comparison.

assumed that the reductive decomposition of the metal nitrates does not lead to a reduction of the Co(II) or Fe(III), respectively. Martens et al. [30] reported that reductive decomposition of residual $Co(NO_3)_2$ resulted in CoO, NO_x and H_2O, hence not lowering the oxidation state of Co(II).

Generally, for the Co-rich samples (Fig. 2), Fe incorporation shifts the low-temperature peak of 0Fe-100Co (a) to slightly higher temperatures (i.e. 650 K → 664–674 K), and the high-temperature peak to lower temperatures (i.e. 930 K → ~895 K). The replacement of 5% of the Co with Fe (catalyst b), however, did not notably affect the position of the high-temperature peak, as shown in Fig. 2B where the TPR patterns of catalyst (a) and (b) are compared. This is in agreement with a lower degree of reduction of catalyst (b) compared to (a) and (c), as measured by PO (see Table 1).

For the Fe-rich samples (Fig. 3), Co incorporation shifts the low-temperature peaks to lower temperatures (e.g. 640 K → 615 K for the $Fe_2O_3 \rightarrow Fe_3O_4$ reduction by replacing 25% of the Fe with Co). Also the high-temperature peak at 1035 K for 100Fe-0Co (g) is shifted to lower temperature (910 K).

All catalysts show broad peaks at temperatures above 1100 K, indicating Al-containing spinels or other Al-Co or Al-Fe species, either present in the calcined sample or formed during the TPR experiment [18,29]. (As to Fe-Co spinels, they should reasonably be reduced as easily as (or more easily than) the pure metal oxides (Co_3O_4 or Fe_2O_3/Fe_3O_4), since the spinel/inverse spinel structure does not in itself imply a low reducibility (both Co_3O_4 and Fe_3O_4 are spinels) [31]). Especially the high-iron content bimetallic catalysts (e and f) show a significant H_2 uptake centred around 1200 K, indicating that a large fraction of the cobalt and iron is present as hard-to-reduce species, probably formed during TPR, which has been reported earlier [11] for bimetallic Fe-Co/TiO_2 catalysts. As shown by XRD and PO measurements (see Section 3.1.5 and Table 1), however, it is mainly catalyst 100Fe-0Co (g) that contains hard-to-reduce species after ordinary reduction (16 h at 623 K), and obviously these species are not even fully reduced during TPR conditions as shown by the comparatively small high-temperature peak area of this catalyst.

By comparing the TPR patterns of 100Fe-0Co (g) and 75Fe-25Co (f), as shown in Fig. 3F, it is clear that the total H_2 uptake of the latter is higher even though catalyst (f) theoretically requires a lower amount of H_2 for complete reduction (2.92 mol H/mol CoFe, see Table 2) than catalyst (g) (3.0 mol H/mol Fe). A higher total H_2 uptake during TPR indicates either a higher oxidation state in the calcined sample, or that the extent of formation of hard-to-reduce species during calcination or TPR is smaller. Most probably, incorporation of Co in the Fe-catalyst results in a weaker chemical interaction between iron and γ-Al_2O_3, which makes the catalyst less prone to form hard-to-reduce Fe-Al species during TPR. As is shown in Section 3.1.5, it is also probable that the calcined catalyst (f) has a higher oxidation state than when assuming only pure metal oxides (Co_3O_4 and Fe_2O_3).

The fact that 100Fe-0Co (g) has a higher H_2 uptake (0.76 mol H/mol Fe) at temperatures below 800 K than 75Fe-25Co (f) (0.58 mol H/mol FeCo) supports the theory that it is during TPR that the hard-to-reduce phases are formed for catalyst (g), and not during calcination. As mentioned above, it is true that a pure Fe catalyst requires larger amounts of H_2 for complete reduction than 75Fe-25Co (f), assuming only Fe_2O_3 and Co_3O_4 present. However, the low-temperature H_2 uptake of 75Fe-25Co (f) is much too low compared to that of 100Fe-0Co (g) to be explained only by the lower Fe content. A plausible explanation for the higher H_2 uptake at temperatures below 800 K for 100Fe-0Co (g) could be that the presence of Co affects the stability of FeO and therefore shifts part of the reduction to higher temperatures. Cobalt in the Fe-rich samples is mixed into the Fe_2O_3 on an atomic level, as shown by XRD (see Section 3.1.5).

Fig. 1C compares the TPR pattern of 75Fe-25Co (f) with that of bulk Fe_2O_3, and it is obvious that the similarity is higher for this pair of curves than for 100Fe-0Co (g) and bulk Fe_2O_3 (Fig. 1B), again pointing in the direction that Co weakens the iron-support interaction taking place at high temperatures in a reductive atmosphere. This interpretation is also supported from the higher degree of reduction (as measured by PO) of catalyst (f) compared with (g) (see Table 1).

3.1.2.3. Degree of reduction of the catalyst samples during TPR. Table 2 shows the theoretical amounts of hydrogen needed for complete reduction of the catalyst samples, assuming only pure metal oxides (Co_3O_4 and Fe_2O_3) in the calcined samples, and also the actual hydrogen uptakes during the TPR. The H_2 uptakes have been corrected for the contribution of the reductive decomposition of the residual nitrates to the TCD signal. The sample weights of approximately 0.2 g have not been corrected for the fact that not all Co and Fe are present as oxides, but some minor parts as nitrates.

Generally, the ratio *actual H_2 uptake:theoretical H_2 uptake* ("degree of reduction during TPR" in Table 2) during TPR increases with the Co content. This was also observed by Brown et al. [29] for a series of Fe-Co-Al (2.5 wt% Al_2O_3) catalysts in the range 40Fe-60Co to 0Fe-100Co, and interpreted as Co increased the Fe(II)/Fe(III) ratio, i.e. reduced the oxidation state and hence the H_2 needed for complete reduction of the calcined catalyst, by the formation of Fe-Co spinels [29,32]. This interpretation is reasonable if the cobalt/iron in the catalysts is fully reduced during the TPR, which was assumed due to the low content of Al_2O_3 in the catalysts. In the present study, however, in which the γ-Al_2O_3 amounts to 88 wt%, a complete reduction of the cobalt and iron during TPR is not as likely, and therefore a lower H_2 uptake during TPR than theoretical is rather interpreted as a sign of an incomplete reduction of the metal oxides due to strong interaction with the support, or due to the formation of hard-to-reduce Fe-Al or Co-Al species, most probably during the TPR. Furthermore, as discussed in Section 3.1.5, no clear evidence of Fe-Co spinels in the calcined samples was found by XRD measurements. The more or less linear trend in "degree of reduction during TPR" with the Fe:Co ratio is consistent with the fact that iron is more difficult to reduce than cobalt, as seen from for instance the TPR patterns of the bulk

Table 2
Quantitative TPR results.

Catalyst	Theoretical H_2 uptake for total reduction [mol H/mol FeCo]	Measured H_2 uptake during TPR [mol H/mol FeCo]	Degree of reduction during TPR [%]	Expected degree of reduction during TPR if physical mixture of (a) and (g) [%]
0Fe-100Co (a)	2.67	2.47	92.5	–
5Fe-95Co (b)	2.69	2.44	90.8	91.3
15Fe-85Co (c)	2.72	2.42	89.0	88.8
25Fe-75Co (d)	2.76	2.18	79.0	86.3
50Fe-50Co (e)	2.84	2.39	84.2	80.1
75Fe-25Co (f)	2.92	2.24	76.9	73.8
100Fe-0Co (g)	3.00	2.03	67.6	–

Table 3
Atomic concentrations of Fe and Co as measured by XPS for three catalysts (b–d).

Catalyst	Atomic Fe/Co concentration [%]				
	Calcined	Reduced (as is)	Reduced, sputtering 100s	Reduced, sputtering 200s	Reduced, sputtering 300s
5Fe-95Co (b)[a]	15/85	–	–	–	–
15Fe-85Co (c)[b]	41/59	40/60	28/72	22/78	18/82
25Fe-75Co (d)[b]	55/45	52/48	48/52	47/53	45/55

[a] The relative uncertainty for the Fe concentration is estimated to ±30%.
[b] The relative uncertainty for the Fe concentration is estimated to ±10%.

materials in Fig. 1. It also suggests that the interaction between the metal and the support increases with the Fe:Co ratio.

Catalyst 25Fe-75Co (d) is deviating from this trend, as shown in Table 2. Furthermore, its H_2 uptake is significantly lower than what is expected from a physical mixture of the pure Fe and pure Co catalysts with the same Fe:Co ratio. The reason for this low H_2 uptake is most probably neither due to a low oxidation state in the calcined catalyst, as discussed above, nor due to a more pronounced interaction between the metals and support. A more probable explanation could be an extensive surface enrichment of Fe, occurring at this particular Fe:Co ratio, which is discussed in Section 3.1.4. Catalysts 50Fe-50Co (e) and 75Fe-25Co (f) both have H_2 uptakes higher than what is expected from a physical mixture of the pure Fe and pure Co catalysts. These features are probably due both to high oxidation states of the calcined samples (see Section 3.1.5), and due to higher degrees of reduction as measured by PO (see Table 1).

3.1.3. Pulse oxidation (PO)

The results from the pulse oxidation indicate that the degree of reduction of a Co/γ-Al_2O_3 catalyst can be slightly increased when incorporating small amounts of Fe (catalyst c). That small amounts of Fe may increase the reducibility of Co has also been reported for bimetallic Co-Fe/TiO_2 catalysts [11]. In the present study, the incorporation of 5% Fe in the Co catalyst, however, resulted in a slightly decreased reducibility (catalyst 5Fe-95Co (b)).

Similar to the results by Duvenhage and Coville [14], the reducibility of catalyst 25Fe-75Co (d) surprisingly drops far below that of the pure Co catalyst (a), while catalyst 50Fe-50Co (e) attains almost the same degree of reduction as the pure Co catalyst (a). Duvenhage and Coville [11] reported that upon reduction for 16 h at 623 K in H_2 of a 5 wt% Fe/5 wt% Co/TiO_2 catalyst (prepared by incipient wetness co-impregnation with the metal nitrates), a bcc FeCo alloy was formed and essentially all metal in the catalyst was fully reduced. The reducibilities for the Fe-Co bimetallic catalysts in the present study are much lower, probably due to a stronger interaction between the metals and the support, but the significant increase in degree of reduction going from 25Fe-75Co (d) to 50Fe-50Co (e) could be explained by the formation of a FeCo alloy in the latter (see Section 3.1.5).

The pulse oxidation results also show that the degree of reduction of a Fe/γ-Al_2O_3 catalyst is significantly increased when incorporating moderate amounts of Co, and hence the large difference in TPR patterns of 100Fe-0Co (g) and 75Fe-25Co (f), as discussed in Section 3.1.2, is reflected in the pulse oxidation results.

The fact that similar trends in reducibility are achieved for γ-Al_2O_3 (present study) and TiO_2-supported catalysts [11,14] (note that different calcination and reduction temperatures are used in [11] and [14]), indicates that this somewhat irregular trend is mainly an effect of the Fe:Co ratio. The surprisingly low degree of reduction of catalyst 25Fe-75Co (d) correlates well with the low H_2 uptake during TPR for this catalyst. The reason for the low degree of reduction for catalyst (d) could be a pronounced surface enrichment of Fe [11]. The slightly lowered reducibility of 5Fe-95Co (b) compared with that of the pure Co catalyst (a) might have the same explanation.

3.1.4. X-ray photoelectron spectroscopy (XPS)

Table 3 shows the results of the atomic concentration measurements by XPS. A clear surface enrichment of Fe is observed for all studied bimetallic samples, i.e. catalysts (b–d). Catalyst 5Fe-95Co (b) seems to have a much lower surface concentration of Fe than 15Fe-85Co (c), although having the same "failed" chemisorption results (see Table 1). This is perhaps explained by the fact that only 10–15% of the XPS signal emanates from the outermost atomic layer, which implies that the contribution from this layer to the total measured concentration is underestimated.

The concentration profiles of the cobalt/iron particles in catalysts 15Fe-85Co (c) and 25Fe-75Co (d) are very different. After 300 s of sputtering, the concentrations in catalyst (c) are similar to the nominal ones, while those for catalyst (d) still indicate enrichment of iron.

Generally, the XPS measurements resulted in broad peaks, indicating that the samples were charged despite the use of a neutralizing ion gun, probably due to lateral variations in conductivity. Peak broadening may also arise from a mixture of different oxidation numbers of the Co or Fe. Only for the reduced 15Fe-85Co (c), clear metallic Co peaks were obtained indicating that this sample possesses distinct areas of metallic Co. Fig. 4 shows the Co 2p XPS spectra for catalysts (c) and (d). It seems as if the Co in the reduced sample (c) is significantly more reduced than the Co in the reduced sample (d). This can explain the large difference in degree of reduction between these samples, as measured by PO. The XPS results hence indicate that a thick iron-rich layer on the surface of the Fe-Co particles inhibits the reduction of the cobalt oxide in the same layer and therefore also in the underlying layers. Fig. 4 also reveals that surface re-oxidation occurred when transferring the samples from the H_2 atmosphere to the UHV chamber.

As to the oxidation state of iron, the low S/N ratio of the spectra limits the useful information. However, the spectra suggest that in the reduced samples, iron is present as a mixed oxide with both oxidation states +II and +III, and possibly also as some metallic Fe. Absence of well-defined metallic Co peaks in the spectra of samples 0Fe-100Co (a) and 5Fe-95Co (b) (not shown) points in the direction that these samples are less reducible compared to 15Fe-85Co (c), which was also found by PO.

3.1.5. X-ray diffraction (XRD)

3.1.5.1. Calcined samples. The XRD patterns for the calcined catalysts are depicted in Fig. 5. The peaks in the 0Fe-100Co (a) and 100Fe-0Co (g) patterns confirm that Co is present as crystalline Co_3O_4 (fcc, e.g. PDF: 74-1657) and Fe as crystalline α-Fe_2O_3 (*hematite*, rhombohedral, e.g. PDF: 84-0307). For the bimetallic catalysts, the Fe_2O_3 phase is clearly visible for the 50% Fe loading and higher Fe loadings. Co_3O_4 and Fe_2O_3 as the only detectable phases by XRD have been reported for a calcined

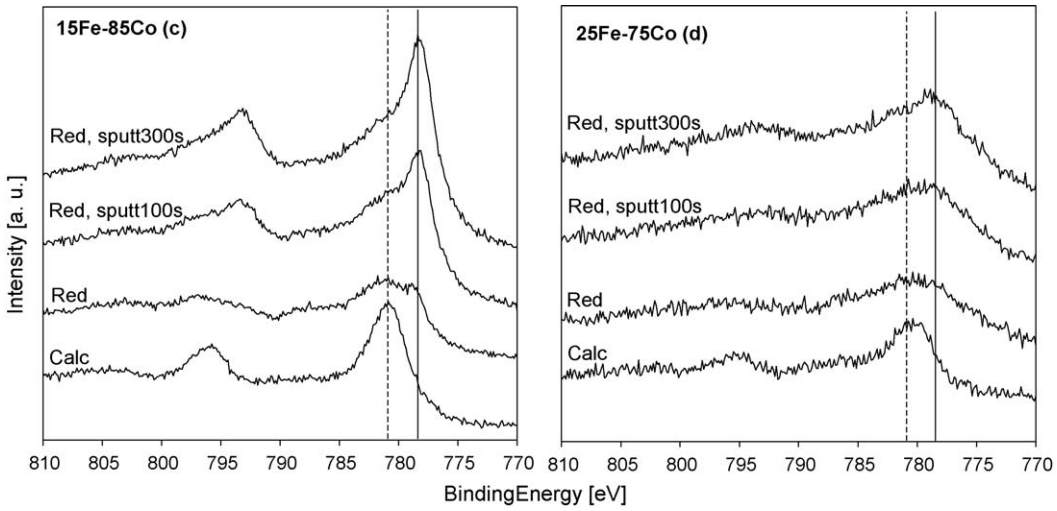

Fig. 4. Co 2p XPS spectra for 15Fe-85Co (c) and 25Fe-75Co (d) after different treatments (Calc = calcined catalyst, Red = after reduction, Red, sputtXs = reduced catalyst after Ar^+ sputtering for Xs). Dashed vertical lines indicate position for oxidized Co. Solid vertical lines indicate position for metallic Co.

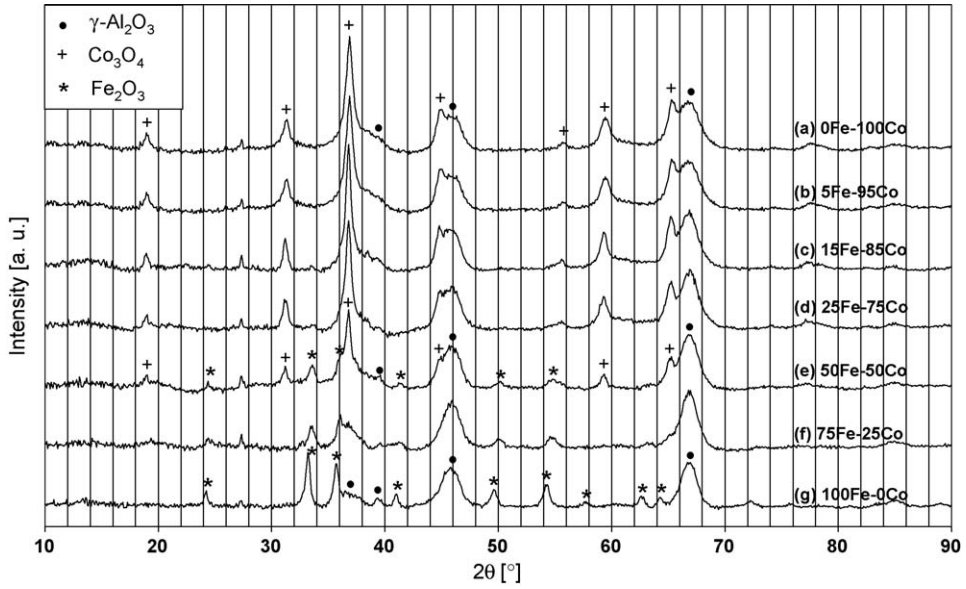

Fig. 5. X-ray diffractograms of the calcined catalysts.

10 wt% Fe/10 wt% Co/TiO_2 catalyst [11]. Brown et al. [29] suggested that there is probably no residual Fe_2O_3 present in bimetallic Fe-Co catalysts with Fe content less than 40%; all the iron in these materials being in the form of Fe-Co spinels. This observation was, however, made for co-precipitated Fe-Co-Al catalysts in which the final catalyst contained only 2.5 wt% of Al_2O_3. As ternary oxides of Co and Fe preferentially form the spinel (or inverse spinel) structure [33], it makes sense to search for Fe-Co spinels in the X-ray diffractograms of the calcined catalysts, as the formation of these spinels would indicate a good mixing degree of the two metals.

The iron-rich Fe-Co spinels (Fe_2CoO_4 or $CoFe_2O_4$, PDF: 22-1086) almost exactly match the diffraction pattern of Fe_3O_4 (*magnetite*, fcc, e.g. PDF: 19-0629). The cobalt-rich Fe-Co spinels (Co_2FeO_4 or $FeCo_2O_4$) have diffraction peaks appearing approximately 1° to higher 2θ compared to the iron-rich Fe-Co spinel [31,34], and approximately 1° to lower 2θ compared to Co_3O_4 [34]. No peaks at the positions where Fe-Co spinels would be expected are visible from the XRD of the calcined samples (Fig. 5). However, for the bimetallic samples with clearly detectable iron content (i.e. e and f) the peaks of Fe_2O_3 were shifted to higher 2θ compared with the pure iron catalyst (g) (see Table 4). This indicates that Co is incorporated into the α-Fe_2O_3, contracting this crystal lattice (since the Co(III) ion is smaller than the Fe(III) ion) and hence shifting the peaks to higher 2θ, as shown in Table 4. The fact that cobalt in these catalysts is more often present as Co(III) than in pure Co_3O_4 (Co(II) and Co(III)) could imply a higher oxidation state in the calcined catalyst, and hence a higher H_2 uptake, than expected from the assumption of the pure metal oxides (Co_3O_4 and Fe_2O_3).

The position of the 100% Co_3O_4 diffraction peak is relatively constant throughout the catalyst series (see Table 4). However, since Co_3O_4 contains both Co(II) and Co(III) it would theoretically be possible to exchange these ions with Fe(II) and Fe(III), respectively, resulting in a broadening of the Co_3O_4 peak, but not a shift in the 2θ position, due to the differences in ionic radii. However, no such broadening, compared to the pure Co catalyst (a), was visible (see Co_3O_4 particle size estimation in Table 1) and hence there is no evidence for Fe being incorporated into the Co_3O_4 phase.

Table 4
2θ values and corresponding d-spacings for the Co_3O_4 and Fe_2O_3 phases of all catalysts. References for Co_3O_4 and Fe_2O_3 are PDF 74–1657 and 84–0307, respectively.

Catalyst	2θ (d-spacing) for the 100% peak of Co_3O_4 (ref. 36.93 and 2.432 Å)	2θ (d-spacing) for the 100% peak of α-Fe_2O_3 (ref. 33.24 and 2.693 Å)
0Fe-100Co (a)	36.76 (2.443)	–
5Fe-95Co (b)	36.88 (2.435)	Not detectable
15Fe-85Co (c)	36.80 (2.440)	Not detectable
25Fe-75Co (d)	36.80 (2.440)	Not measurable
50Fe-50Co (e)	36.76 (2.443)	33.64 (2.662)
75Fe-25Co (f)	Not measurable	33.48 (2.674)
100Fe-0Co (g)	–	33.24 (2.693)

The shift in the positions of the α-Fe_2O_3 peaks, as shown in Table 4, is most apparent comparing catalyst 100Fe-0Co (g) and catalyst 75Fe-25Co (f), clearly indicating the incorporation of Co into the Fe_2O_3 lattice. This clear difference between catalyst (f) and (g) was also seen in the TPR, and the shift of all TPR peaks of 100Fe-0Co (g) to lower temperatures upon replacing 25% of the Fe with Co mentioned above is therefore probably connected to this Fe-Co mixed phase.

The average particle sizes of Co_3O_4 and Fe_2O_3, when possible to estimate, of the calcined samples (see Table 1) are similar for catalyst (a) to (f). For the 100% Fe catalyst (g), however, the particle size of Fe_2O_3 is somewhat larger, implying that incorporating Co into the Fe_2O_3 phase reduces the size of the corresponding crystallites.

As to the spinels containing aluminum, the resolution limitations of the X-ray diffractograms make it impossible to distinguish the $CoAl_2O_4$ and Co_2AlO_4 from Co_3O_4, due to the very close resemblance in diffraction patterns. Exact phase determination of the catalysts is, however, outside the scope of this paper. The Fe-Al spinels ($FeAl_2O_4$ and Fe_2AlO_4) both contain Fe(II) and are hence not likely to form during calcination. In any case, $FeAl_2O_4$ (PDF: 34-0192) would be clearly visible in XRD since its diffraction pattern clearly deviates from those of Fe_2O_3 (and also from that of Fe_3O_4). Fe_2AlO_4 should according to Walsh et al. [33] have a similar diffraction patterns as Fe_3O_4, only shifted slightly to higher 2θ. No Fe-Al spinels are visible in the XRD of the calcined samples.

3.1.5.2. Reduced and passivated samples. Fig. 6 shows the X-ray diffractograms of the reduced and passivated samples. The reduction and passivation of the 0Fe-100Co (a) sample resulted in only CoO as detected by XRD, while that of the 100Fe-0Co (g) sample resulted in both metallic Fe and a phase with a diffraction pattern closely resembling that of Fe_3O_4. As to the pure Co catalyst (a), it is obvious that the passivation procedure was not able to protect the formed metallic Co. The 100% peak of the most stable form of Co crystallites smaller than 100 nm [35] (fcc, PDF: 15-0806) would appear at $2\theta = 44.21°$ (partly overlapped by the broad γ-Al_2O_3 peak). If the reduction only resulted in CoO, the degree of reduction would only be 25%. The value obtained by pulse oxidation was 49% (see Table 1) which is significantly higher and therefore confirms that metallic Co is present in the reduced catalyst. For reduced and passivated sample 25Fe-75Co (d), a small shoulder at $2\theta = 44–45°$, indicates the presence of a larger amount of metallic phase, and hence a more successful passivation in the presence of iron. It is not easy to determine the composition of this metallic phase since the strongest Fe(0) peak (bcc, PDF: 6-0696, 100% peak at $2\theta = 44.68°$) lies close to that of Co(0) or that of FeCo alloy (bcc, 100% peak slightly shifted to higher 2θ compared to Fe(0)). It is probably Co(0) since the concentration of Fe is very low and all Fe-containing phases would give very low intensities. An FeCo alloy is possible judging solely from the XRD pattern, but the low degree of reduction as measured by PO for this catalyst, and the high reducibility reported for bimetallic Fe-Co catalysts forming FeCo alloys upon reduction [11], speak for Co(0).

Looking at the highest metallic Fe (bcc) diffraction peak not overlapped by the peaks of γ-Al_2O_3, i.e. at $2\theta = 82.33°$, for samples (e–g) in Fig. 7 it seems as if this peak is shifted slightly towards higher 2θ with a higher Co content, which is indicative of an FeCo alloy (Fe-rich). This somewhat vague indication, together with the clear evidence of the presence of a mixed Fe-Co phase in the calcined samples (i.e. Co incorporated into Fe_2O_3), points in the direction of the formation of an Fe-rich FeCo alloy upon reduction of the calcined Fe-rich samples. From Fig. 7 it can also be seen that the "alloy" peak width is broader the higher the Co content of the catalyst, implying that cobalt increases the dispersion of iron. Duvenhage and Coville [11] found that pure Co on TiO_2 existed as fcc or hcp, while pure Fe on TiO_2 as bcc. Their 5 wt% Fe/5 wt% Co/TiO_2 catalyst had a bcc alloy of Co and Fe, while in lower Fe content

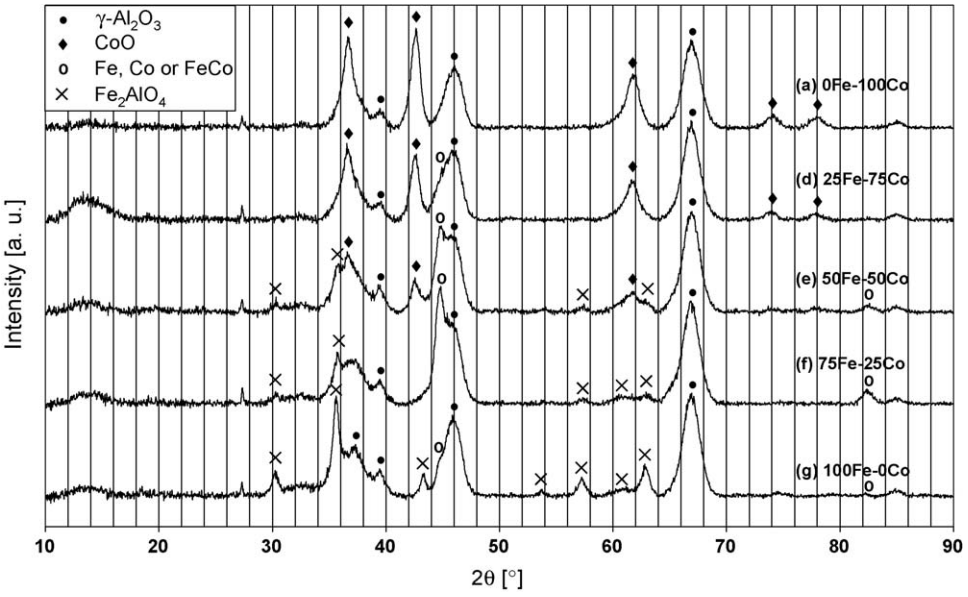

Fig. 6. X-ray diffractograms of selected reduced and passivated catalysts.

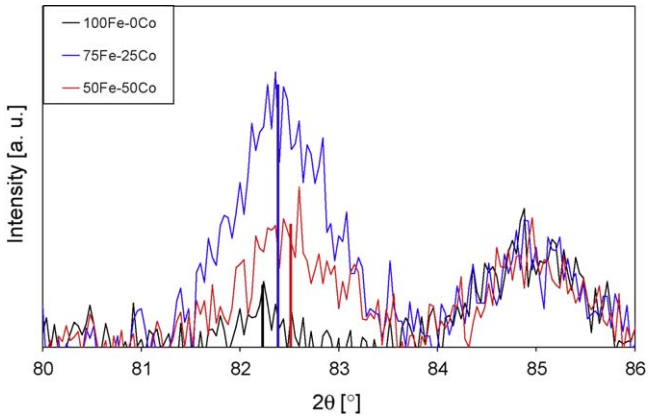

Fig. 7. Selected part of the X-ray diffractograms of reduced and passivated iron-rich catalysts (e–g). The peaks centered between $2\theta = 82–83^\circ$ correspond to FeCo alloys.

catalysts the Co fcc structure was retained and Fe segregated to the surface of the bimetallic system.

Investigating the Fe_3O_4-similar phase of 100Fe-0Co (g) more closely, it is found that the peaks are shifted slightly to higher 2θ compared to those of Fe_3O_4. This could indicate that Fe_2AlO_4 has formed during the reduction, as discussed above, since it is not probable that this phase should be a result of the passivation. The large decrease in the peak intensities of this phase when moving from the pure Fe sample (g) to 75Fe-25Co (f) indicates that cobalt prevents the reaction between the iron and the γ-Al_2O_3 during reduction, hence improving the reducibility of the iron, as seen by the PO results (see Table 1) This might possibly be due to Co(II) showing a high preference for entering the defect spinel structure of γ-Al_2O_3. It has also been reported that cobalt prevents the formation of $FeTiO_3$ for Fe/TiO_2 catalysts [11].

Inherent problems associated with characterization of reduced and passivated samples, as opposed to *in situ* characterization of reduced catalysts, have been discussed previously by Huber et al. [36]. In the present study, the reduced and passivated catalyst sample with the highest metallic content is 75Fe-25Co (f), as visible from Fig. 6. However, the PO results show that this catalyst has a significantly lower degree of reduction compared to for instance that of 50Fe-50Co (e). These observations imply that also for catalyst 50Fe-50Co (e), part of the CoO is a result of the passivation.

3.2. Catalytic reaction

3.2.1. Effect of GHSV and Fe:Co ratio on selectivity and activity

Table 5 shows the CO conversion, space–time yield of hydrocarbons and selectivity to C_{5+} (CO_2-free), CH_4 (CO_2-free) and CO_2 for the different Fe-Co/γ-Al_2O_3 catalysts in the five periods. For catalysts (e–g), only periods 1 and 2 were run.

3.2.1.1. Selectivity. The selectivities to C_{5+}, CH_4 and CO_2 for catalysts with up to 25% Fe content (catalysts a–d) presented in Table 5 show similar trends when the GHSV decreases: the selectivity to C_{5+} increases and the selectivities to CH_4 and CO_2 decrease. Furthermore, the olefin/paraffin ratio of C_3 is reduced, as shown in Table 6. These features are well known for Co-based catalysts [20] and that C_{5+} selectivity increases and the olefin/paraffin ratio of C_3 decreases with lowered GHSV has also been reported for Fe-based catalysts [37,38]. However, for the catalysts with the highest Fe content (catalysts f and g), the C_{5+} selectivity is actually decreased when lowering the GHSV, and the selectivity to CO_2 is increased. This increase in selectivity to CO_2 is due to the percentage reduction in space–time yield of CO_2 being lower than the corresponding reduction in space–time yield of hydrocarbons (see Table 5), and not due to an increased space–time yield of CO_2. The reason for a lowered selectivity to C_{5+} with a lowered GHSV

Table 5
Activities and selectivities (C-atom) to C_{5+}, CH_4 and CO_2 for all catalysts in all periods. Average values for each period are given.

Catalyst	Condition	CO conversion [%]	Space–time yield of hydrocarbons [$g_{HC}/g_{cat}.h$]	Space–time yield of CO_2 [$g_{CO2}/g_{cat}.h$]	Selectivity to C_{5+} (CO_2-free) [%]	Selectivity to CH_4 (CO_2-free) [%]	Selectivity to CO_2 [%]
(a) 0Fe-100Co	Dry feed	5.7	0.20	0.022	82.2	8.8	3.4
	Reduced GHSV	23.6	0.21	0.011	86.6	6.0	1.6
	20% water	19.8	0.17	0.015	87.3	4.5	2.5
	33% water	13.6	0.12	0.014	86.4	4.2	3.8
	Dry feed	13.6	0.12	0.010	82.0	7.8	2.7
(b) 5Fe-95Co	Dry feed	7.5	0.27	0.026	78.0	10.1	3.1
	Reduced GHSV	25.4	0.23	0.016	79.7	8.4	2.3
	20% water	20.5	0.18	0.028	83.0	5.4	4.7
	33% water	15.0	0.13	0.018	82.7	5.1	4.3
	Dry feed	17.2	0.15	0.012	80.1	8.1	2.5
(c) 15Fe-85Co	Dry feed	7.2	0.25	0.029	78.2	10.2	3.6
	Reduced GHSV	22.0	0.20	0.018	78.3	9.3	2.9
	20% water	16.9	0.15	0.026	81.8	6.2	5.4
	33% water	12.7	0.11	0.019	81.4	5.9	5.3
	Dry feed	14.4	0.13	0.015	74.8	10.4	3.8
(d) 25Fe-75Co	Dry feed	5.8	0.20	0.033	70.0	13.5	5.1
	Reduced GHSV	20.8	0.18	0.023	72.8	11.3	3.9
	20% water	18.3	0.15	0.049	77.3	7.3	9.3
	33% water	7.7	0.06	0.024	71.3	9.6	10.6
	Dry feed	16.9	0.15	0.023	72.7	11.8	5.0
(e) 50Fe-50Co	Dry feed	4.4	0.15	0.028	64.9	14.8	5.5
	Reduced GHSV	13.8	0.12	0.022	64.8	14.9	5.5
(f) 75Fe-25Co	Dry feed	3.2	0.11	0.029	64.9	15.6	8.1
	Reduced GHSV	7.7	0.06	0.023	48.1	23.1	10.5
(g) 100Fe-0Co	Dry feed	4.5	0.16	0.031	59.2	16.6	6.1
	Reduced GHSV	10.0	0.09	0.025	51.9	20.0	8.7

Table 6
Selectivity to C_3 and olefin/paraffin ratio for C_3 for all catalysts in all periods. Average values for each period are given.

Catalyst	Condition	CO conversion [%]	C_3-selectivity (tot C) [%]			C_3 (olefin/paraffin)
			Olefin	Paraffin	Total	
(a) 0Fe-100Co	Dry feed	5.7	2.7	0.7	3.4	3.6
	Reduced GHSV	23.6	2.3	0.7	3.0	3.4
	20% water	19.8	2.7	0.6	3.2	4.6
	33% water	13.6	3.0	0.6	3.6	5.0
	Dry feed	13.6	3.2	0.9	4.1	3.5
(b) 5Fe-95Co	Dry feed	7.5	3.4	1.0	4.4	3.3
	Reduced GHSV	25.4	3.3	1.3	4.6	2.6
	20% water	20.5	3.4	0.9	4.3	3.9
	33% water	15.0	3.7	0.9	4.5	4.3
	Dry feed	17.2	3.5	1.1	4.6	3.2
(c) 15Fe-85Co	Dry feed	7.2	3.3	1.0	4.3	3.3
	Reduced GHSV	22.0	3.5	1.3	4.9	2.6
	20% water	16.9	3.6	1.0	4.5	3.7
	33% water	12.7	3.7	0.9	4.7	4.0
	Dry feed	14.4	4.2	1.5	5.7	2.8
(d) 25Fe-75Co	Dry feed	5.8	4.6	1.5	6.1	3.2
	Reduced GHSV	20.8	4.3	1.8	6.2	2.4
	20% water	18.3	4.3	1.2	5.6	3.5
	33% water	7.7	4.7	1.5	6.1	3.2
	Dry feed	16.9	4.0	1.8	5.8	2.2
(e) 50Fe-50Co	Dry feed	4.4	4.9	1.6	6.6	3.1
	Reduced GHSV	13.8	5.0	2.3	7.3	2.1
(f) 75Fe-25Co	Dry feed	3.2	4.1	1.6	5.7	2.6
	Reduced GHSV	7.7	6.2	3.3	9.5	1.9
(g) 100Fe-0Co	Dry feed	4.5	5.1	2.1	7.2	2.4
	Reduced GHSV	10.0	5.7	3.5	9.2	1.7

could possibly be that at high Fe content, the FT-active phase of the catalyst is rapidly oxidized at higher water partial pressures (higher conversions). An increase in the relative production of gaseous products with the time-on-stream for a 5 wt% Fe/5 wt% Co/TiO_2 catalyst due to deactivation has been reported [14]. In the present study, however, the deactivation rate in period 1 and 2 was similar for all catalysts. Another, more plausible, explanation could be that for catalysts (f) and (g), the H_2/CO ratio inside the reactor increases from period 1 to 2 due to the increased selectivity to CO_2, and hence the selectivity to more hydrogenated products (shorter HCs) increases.

Regarding the absolute values of the selectivities, it is possible to directly compare them between catalysts (a–d) in periods 1 and 2 because the conversion levels are very similar. Table 5 shows that the higher the Fe content, the shorter the formed hydrocarbons. Ishihara et al. [15] also found an increasing selectivity to CH_4 with increasing Fe content in $Fe-Co/SiO_2$ catalysts. Pure Fe catalysts without alkali promotion have poor chain-growth probabilities, which could be the explanation for this finding [4]. The high Fe content of catalysts (e–g), together with the low conversion levels, result in very low selectivities to C_{5+} in period 1 (see Table 5). This is not in agreement with Ishihara et al. [15] who obtained a significantly higher C_{6+} selectivity for a 75 mol% Fe/25 mol% Co/SiO_2 catalyst compared to a pure Co/SiO_2 catalyst (523 K, 10 bar, $H_2/CO = 1.9$). Similarly, Arai et al. [17] reported a significantly higher C_{6+} selectivity for a 5 wt% Fe/5 wt% Co/TiO_2 catalyst compared to a 10 wt% Co/TiO_2 (523 K, 10 bar, $H_2/CO = 1.9$). In these two studies [15,17], however, the conversion levels of the bimetallic catalysts referred to above were higher (due to higher activities) compared to the pure Co catalysts, which might explain part of the higher selectivities to C_{6+}. Duvenhage and Coville [14] generally obtained a lower C_{5+} selectivity the higher the Fe content, except for the 5 wt% Fe/5 wt% Co/TiO_2 catalyst that had a higher selectivity than the 2.5 wt% Fe/7.5 wt% Co/TiO_2 catalyst which was surface-enriched in iron. It is not easy to decide whether this trend [14] is a result of different conversion levels or not.

The higher the Fe content, the lower is the olefin/paraffin ratio for C_3 (Table 6). In LTFT, Fe-based catalysts are known to mainly produce paraffinic wax, just as Co-based catalysts [9]. At higher temperatures and if promoted by K [39] and/or Mn [9], Fe-based catalysts give highly olefinic products. Also the acidity of the support material may affect the olefin/paraffin ratio and the chain-growth probability of supported iron-based catalysts, a higher acidity (e.g. Al_2O_3) resulting in lower olefin/paraffin ratio and lower selectivity to C_{5+} [40]. Amelse et al. [16] reported a significant increase in olefin/paraffin ratio for C_3 for a $Fe-Co/SiO_2$ catalyst compared to the pure Fe and Co catalysts, at a reaction temperature of 523 K. Also Duvenhage and Coville [14] obtained a higher fraction of olefins for their 75Fe-25Co (26.9%) and 50Fe-50Co (15.8%) TiO_2-supported catalysts as compared with pure Fe (0%) and Co (3.8%) catalysts, at a reaction temperature of 493 K. It is probable that the lower inlet H_2/CO ratio in the present study partly contributes to the trend in decreased olefin/paraffin ratio with increased Fe-content. This, again, is explained by a higher H_2/CO ratio inside the reactor for the catalysts with higher selectivity to CO_2.

Similarly to the results of Duvenhage and Coville [14], the pure Fe catalyst (g) gives the lowest olefin content in the products at relatively low FT synthesis temperatures (483–493 K), which was explained by the low degree of reduction [14].

3.2.1.2. Activity. The Fe-containing catalysts (b–g) show a decrease in the space–time yield of hydrocarbons with a decrease in GHSV (Table 5), whereas the Co/Al_2O_3 (a) catalyst shows a slight increase in FT activity. Fe-based catalysts typically lose FT activity upon a reduction in GHSV due to the kinetic rate being inhibited by the water pressure, whereas the kinetic reaction rate of Co-based catalysts has been reported to be rather unaffected or even

positively affected by this reaction product [3,5,20,41]. The results indicate that even for a low Fe:Co ratio, a major part of the FT activity is emanating from the Fe, consistent with a surface enrichment of Fe. It should be mentioned though that Botes and Breman [6] recently presented a FT reaction-rate expression for Fe-based catalysts without including the partial pressure of water. Assuming that water does not inhibit the reaction rate, the reason for a lower space–time yield of hydrocarbons for the Fe-containing catalysts at a lower GHSV (i.e. at a higher conversion) could be a higher sensitivity to a reduction in partial pressure of syngas as compared to Co catalysts.

From Table 5 and Fig. 8 it is obvious that, generally speaking, replacing a large fraction of the Co with Fe (catalysts e–g) results in markedly lowered FT activity, consistent with a lower site activity of Fe as compared to Co [42]. From the CO conversion in period 1 and 2 in Fig. 8 it is clear that the total FT activity of catalysts (a–d), however, show a non-linear trend in FT activity vs. Fe content, which could be explained by different degrees of Fe-Co interaction and thus by different reducibilities, metal dispersions, Fe surface enrichment and site activities for FT and WGS [11,14]. The replacement of Co with small amounts of Fe (5 –15%) improves the FT activity at dry conditions and low conversions (i.e. period 1), and it is believed that this is due to a slightly higher activity of the Fe-Co mixture, as found by others [11,15], and not due to an increased relative WGS activity. This could be concluded from that the Fe-Co catalyst (b) actually has a higher usage ratio (i.e. lower relative WGS activity) than the pure Co catalyst (a). Duvenhage and Coville [11] reported an increase in total activity (reduction in H_2 at 623 K for 16 h, syngas $H_2/CO = 2$) upon co-impregnation of a small amount of Fe (0.1 wt%) to 10 wt% Co/TiO_2, which was due to an increased number of active sites.

Ishihara et al. [15] reported a higher total activity (reduction in H_2 at 523 K for 1 h, syngas $H_2/CO = 1.9$) of a 10 wt% bimetallic Fe-Co/SiO_2 catalyst compared with a 10 wt% Co/SiO_2 for investigated Fe contents between 25 and 75 mol% of the bimetal, but with TiO_2 as support [17] this positive alloying effect was only found for a 50Fe-50Co sample (not for 25Fe-75Co or 75Fe-25Co). In agreement with the present study, Duvenhage and Coville [14] obtained (for similar Fe-Co loadings and ratios as Ishihara et al. [15]) lower total activities (and site activities) for the bimetallic catalysts compared to a Co/TiO_2 catalyst, but their 50Fe-50Co catalyst showed higher activity than either the 25Fe-75Co or 75Fe-25Co, as a result of an extensive iron surface enrichment in 25Fe-75Co. Catalyst 50Fe-50Co (e) in the present study shows a lower FT activity compared to catalyst 25Fe-75Co (d) despite the higher reducibility and higher WGS-selectivity of the former, probably due to even more Fe on the surface of 50Fe-50Co (e) and no positive effect from the FeCo alloy.

The activity trend among the Fe-rich catalysts is also non-linear with respect to Fe content (see Table 5 and Fig. 8). The pure iron catalyst (g) has a higher activity than catalyst 75Fe-25Co (f). This, again, could not be explained by a higher relative WGS activity of the pure Fe catalyst (g), as this actually has a higher usage ratio than catalyst (f). Similar results were reported by Amelse et al. [16] with a 3.85 wt% Fe/1.02 wt% Co/SiO_2 catalyst having significantly lower total activity compared to a pure Fe/SiO_2 catalyst (reduction in H_2 at 698 K for 24 h, syngas $H_2/CO \approx 3$). It has been reported [11,16] that adding small amounts of Co to Fe suppresses the carbide formation. Since iron carbides are the species most frequently reported to be the FT-active phase in iron catalysts [43,44], it is reasonable that such a suppression would result in a lowered activity for a catalyst mainly consisting of iron, despite the

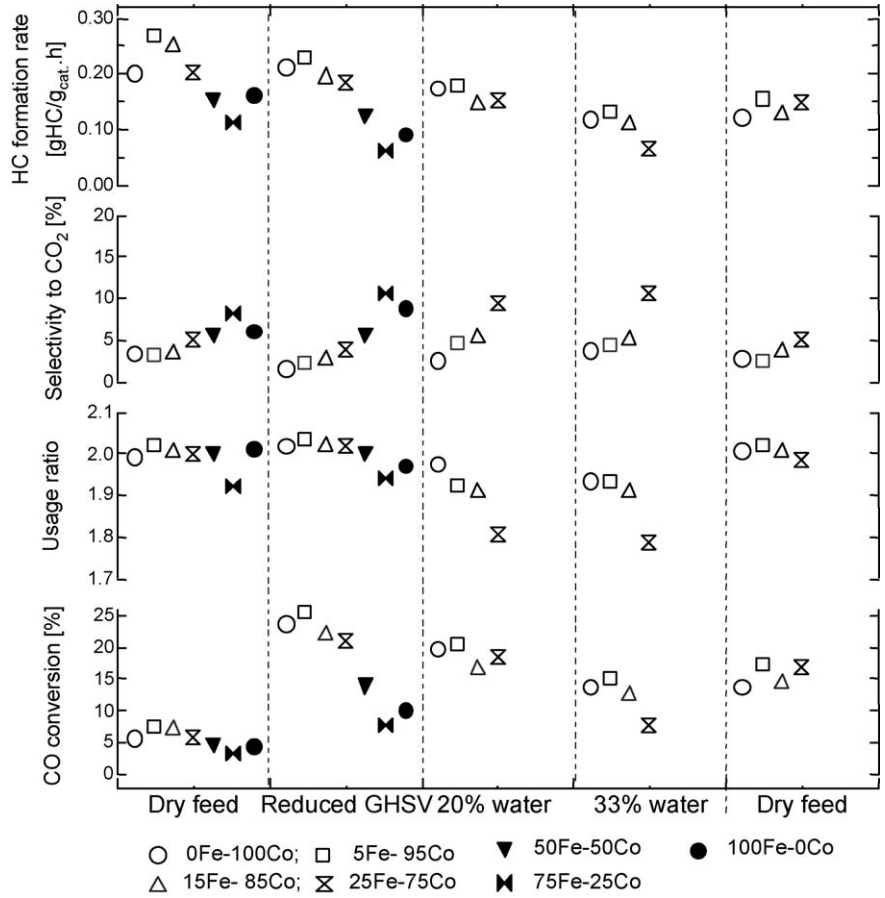

Fig. 8. Average space–time yield of hydrocarbons (HC formation rate), CO_2 selectivity, usage ratio and CO conversion for all catalysts in different periods. Fe:Co ratio increases to the right in each period.

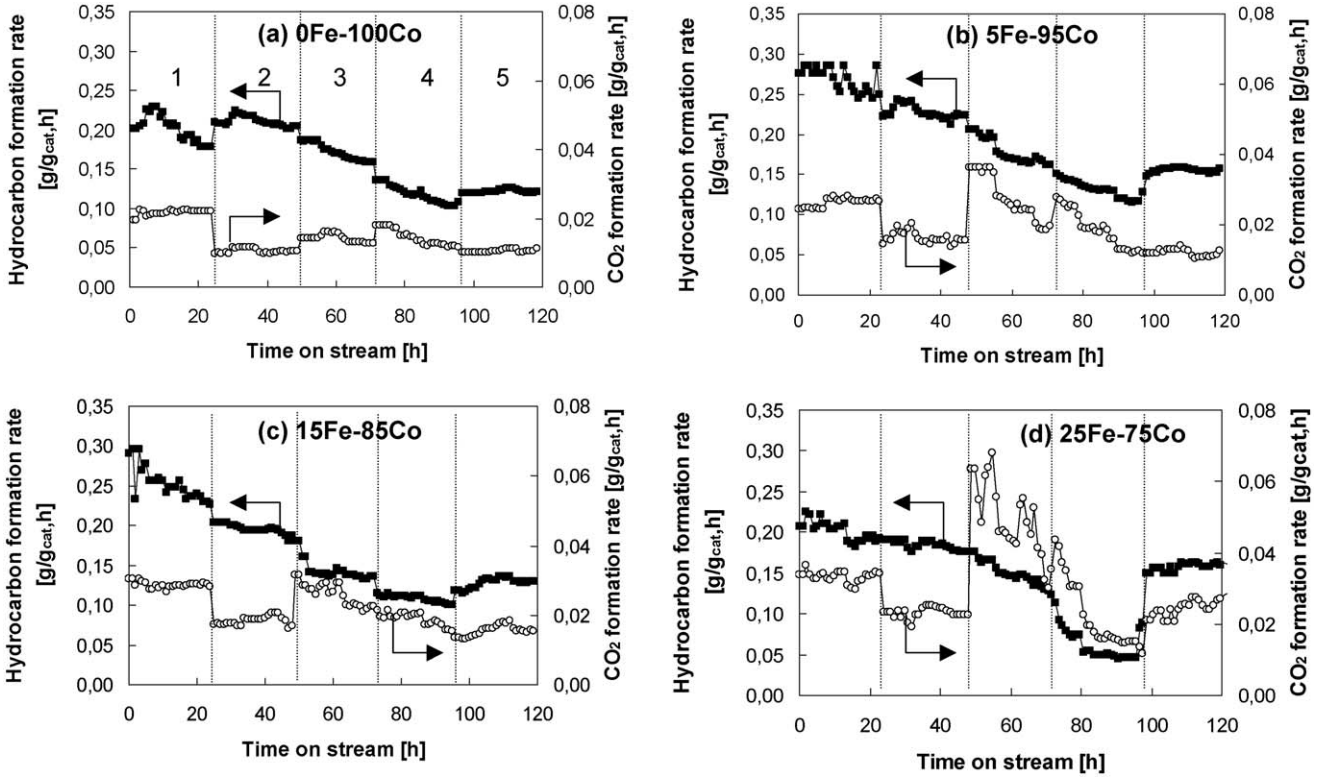

Fig. 9. Space–time yields (formation rates) of hydrocarbons and CO_2 for catalysts (a–d) in different periods.

fact that Co addition improves the degree of reducibility, probably due to a lowered site activity (TOF) [16].

The discrepancies between the reported Fe-Co alloying effects may to some extent be explained by the different reduction conditions used for activation/reduction of the catalysts. It has been reported that activating an iron catalyst in hydrogen renders a catalyst with lower activity compared to activating the catalyst in syngas [45,46]. Bengoa et al. [47] found that for fully H_2-reduced iron catalysts (i.e. only Fe(0) present), only χ-Fe_5C_2 is formed after contact with syngas, but if the H_2-reduction is not complete, some Fe_3O_4 will remain in the sample. Upon contacting with syngas, this Fe_3O_4 will convert into a non-stoichiometric iron carbide ($Fe_{2.4}C$) which is not fully carburized and therefore contains a high number of carbon vacancies giving it higher activity. Hence, different H_2-reduction temperatures and times, as well as different support materials, will give different degrees of reduction of the catalysts, and, accordingly, different iron carbides may form as they are contacted with the syngas. In the presence of Co, the H_2-reduction of iron is enhanced, as shown by TPR, and thus for long H_2-reduction times and high reduction temperatures, the presence of Co might have a negative impact on the type of iron carbide formed. At an incomplete H_2-reduction, however, the presence of Co probably does not affect the carburization of iron and therefore its presence can instead improve the overall activity as Co is known to have much higher site activity than Fe.

Fig. 8 shows that the usage ratios in the dry periods are all very high, which indicates negligible WGS activity for all catalysts. The higher usage ratio and lower selectivity to CO_2 (i.e. lower relative WGS activity) of the pure Fe catalyst (g) in the current study compared with catalyst 75Fe-25Co (f) is in agreement with the results of Amelse et al. [16] for SiO_2-supported catalysts. They attributed this to the inhibition of iron carbide on the FeCo alloy.

Fig. 9 shows the complete "time-on-stream" profiles of space–time yield of hydrocarbons and CO_2 for catalysts (a–d) in the five periods. A common feature for all four catalysts is the decrease in space–time yield of CO_2 as the GHSV is lowered (period 1 → 2). The same is valid for catalysts (e–g) (see Table 5). A first-order dependency of the reaction term, in the rate expression for WGS, on the CO partial pressure over Fe-based catalysts under FT conditions has been reported [48]. The small reduction in CO partial pressure as the syngas conversion is increased (period 1 → 2) is probably enough for a reduction in space–time yield of CO_2.

3.2.2. Effect of water addition and Fe:Co ratio on the FT and WGS activities and hydrocarbon selectivity

The effect of water addition to the feed on the FT and WGS activities and selectivities is illustrated in Tables 5 and 6 and in Figs. 8 and 9. Table 5 shows that water decreases the space–time yield of hydrocarbons and the selectivity to CH_4, but slightly increases the C_{5+} and CO_2 selectivity for both Co and Fe-Co/Al_2O_3 catalysts. For catalyst (d), however, the selectivity to C_{5+} in period 4 drops below that in period 2 due to the severe decrease in CO conversion caused by the high water pressure. Table 6 shows that the olefin/paraffin ratio for C_3 is increased upon water addition, which has been reported previously [20,49].

Part of the reduced space–time yield upon water addition to the feed is due to the lowered syngas partial pressure. However, as Fig. 9 indicates, the decrease in space–time yield of hydrocarbons with added water (in period 4) for catalyst 25Fe-75Co (d) is more pronounced than for the catalysts with lower Fe content. Because the reaction rate is obviously negatively affected by water (alternatively, more sensitive to a reduction in syngas partial pressure), this indicates that a major part of the FT activity for this catalyst comes from the Fe. From Fig. 9 it is clear that the kinetic, i.e. instant, decrease in FT activity when shifting from 20% to 33% steam (period 3 → 4) for catalyst (d) is larger than for the lower Fe-content catalysts (a–c). Furthermore, the deactivation of the FT activity is much faster for catalyst (d) in period 4, which is due to the large part of the FT activity emanating from Fe in this catalyst,

the oxidation of which is a well-known deactivation phenomenon at high water partial pressures [3].

Upon introduction of only 20% water (period 2 → 3), however, catalyst (d) almost retains the FT activity of period 2 due to a relatively high WGS activity keeping the partial pressure of H_2 sufficiently high to overcome the dilution effect of water. Upon introduction of 33% water (period 3 → 4), the negative kinetic effect of water on a catalyst of which the FT activity is mainly Fe-based, cannot be overcome by the WGS activity of the same.

Common for the four catalysts (a–d) in Fig. 9 is the instantaneous increase in space–time yield of CO_2 upon external water addition (period 2 → 3 all catalysts, and 3 → 4 all except for (c)), generally accompanied by a decrease in space–time yield of hydrocarbons. This is probably a purely kinetic effect; the WGS rate is favored at higher external water pressures over the WGS-active sites on the studied catalysts [48], and the FT reaction over the FT-active sites is affected negatively by the lowered syngas pressures and/or by the increased water pressure.

As shown in Fig. 9, the increase in WGS activity upon external water addition is highest for catalysts 5Fe-95Co (b) and 25Fe-75Co (d), indicating more iron on the catalyst surface for these compared to catalyst 15Fe-85Co (c). As discussed above in Sections 3.1.1 and 3.1.3 it is probable that catalyst (b) has a higher degree of Fe surface enrichment than catalyst (c), although having a lower absolute Fe content. It is also possible that the relatively high degree of reduction of catalyst (c) has a negative effect on the WGS activity, oxidized species having a higher WGS-activity as discussed in Section 3.2.3.

As a result of the increased relative WGS activity upon water addition, the usage ratios are lowered (Fig. 8). However, the usage ratios are still far from the desired value of 1.0, i.e. the inlet H_2/CO ratio.

3.2.3. Deactivation and nature of active sites

The deactivation profiles for FT and WGS reactions for catalysts (a–d) can be seen from Fig. 9. Generally, the deactivation rate for the hydrocarbon and CO_2 formation during periods 3 and 4, when water is added externally, is significantly higher than in the dry periods. However, for catalyst 15Fe-85Co (c), no clear successive deactivation in the FT activity was observed in periods 3 and 4. Fe catalysts are known to be more sensitive to re-oxidation than Co catalysts [3], which is a probable explanation for the very rapid deactivation of FT activity of catalyst (d) compared to (a) in period 4. Deactivation of LTFT Fe-based catalysts often proceeds through re-oxidation of the active iron phase into Fe_3O_4, and through sintering of the iron particles [44,50]. However, not only does the space–time yield of hydrocarbons rapidly decrease during period 4 for catalyst (d), but also the space–time yield of CO_2. The fact that the deactivation profiles of the space–time yields of hydrocarbons and CO_2 look very similar makes it tempting to suggest that the FT activity is decreased partly due to the decreased H_2 pressure as the WGS activity declines. However, this effect should only be minor due to the very low extent of WGS. Another explanation for the similar deactivation profiles is that the WGS and FT sites are equally affected by the deactivation process/es.

3.2.3.1. The pure Co catalyst. In the pure Co catalyst (a) it is probably the oxidized surface Co that possesses the WGS activity [51]. Since the formation of oxidized Co is favored during periods 3 and 4, no apparent deactivation of the WGS activity is visible for the Co/γ-Al_2O_3 (a) catalyst in period 3. In period 4, however, a moderate deactivation in both FT activity and WGS activity is visible for catalyst (a), which could be due to a sintering effect. The permanent deactivation of catalyst (a) as to its FT activity is rather severe. The FT activity in period 2 decreased to only 60% in period 5 (both dry periods). Co catalysts are known to deactivate from re-oxidation and sintering of Co particles [3,35]. Turning off the water (period 4 → 5), the space–time yield of CO_2 decreases slightly for catalyst (a) as a result of the lowered water pressure, i.e. a kinetic effect. As opposed to the FT activity, the WGS activity for catalyst (a) is actually slightly increased from period 2 to period 5 despite sintering, probably due to re-oxidation. The severe permanent deactivation of the FT activity and absence of any deactivation on the WGS activity actually imply that both sintering and oxidation must take place, and that it is the oxidized Co that is active for the WGS reaction. Van de Loosdrecht et al. [52] recently reported that only Co crystallites smaller than approximately 5 nm are (surface) oxidized during FT conditions. It is therefore probable that only the smallest Co-particles, i.e. the ones smaller than the average size as measured from XRD, are re-oxidized during the FT synthesis and hence active for the WGS reaction in catalyst (a).

3.2.3.2. The Fe-containing catalysts. For Fe-based catalysts under FT conditions the nature of the WGS-active site is a matter of debate. A typical Fe-based WGS catalyst is composed of Fe_2O_3/Cr_2O_3, which upon controlled reduction in H_2/H_2O mixtures results in the active Fe_3O_4 phase [53]. It has been suggested that Fe_3O_4 is also the WGS-active phase under FT conditions [54], while others claim that it is metallic or carburized Fe [43]. As opposed to the pure Co catalyst (a), for the Fe-containing catalysts (b–d), the space–time yield of CO_2 is rather unchanged or increases slightly upon removal of water from the feed (period 4 → 5). This could not be a kinetic effect for catalysts (b) and (d) since an increase in the space–time yield of CO_2 was observed for these catalysts upon 30% water addition (period 3 → 4). The increase in space–time yield of CO_2 after turning off the water (catalyst d), or the fact that it is not decreasing although the partial pressure of water is lowered (catalysts b and c), is probably due to a regeneration process in which a phase inactive for WGS is reduced into a WGS-active phase. Assuming that Fe_3O_4 is the WGS-active phase, the deactivation upon external water addition must be explained by a change in the formed Fe_3O_4, the favored phase at high water pressures [55], possibly by surface-oxidation into the inactive maghemite (γ-Fe_2O_3) [50,56]. Another option would be deposition of elemental carbon on the WGS-active sites [43].

Comparing the space–time yields of CO_2 in period 2 with those in period 5, i.e. the permanent "deactivation", it is shown in Fig. 9 that the yields are only slightly reduced (catalysts b and c), or even somewhat increased (catalyst d). The permanent deactivation of the FT activities is definitely more pronounced. This observation intuitively suggests a different nature of the active sites for WGS and FT for these catalysts, and that the WGS active sites are oxidized metallic sites (Fe, Co or FeCo). The catalysts contain a larger fraction of these oxidized species after exposure to water compared to in the fresh state.

The results of the present study generally show that the higher the Fe content in the bimetallic catalysts, the higher the relative WGS activity (as illustrated by selectivity to CO_2 in Fig. 8), but the lower the FT productivity. This behavior could indicate a competition between the FT and WGS reactions for the same active sites. However, this is not very likely as discussed above, and as already reported, since the WGS-active phase probably consists of oxidized phases (Fe_3O_4 [54] or CoO [51]), whereas the FT-active phases are iron carbide, metallic Co and/or metallic alloys of Co and Fe [9,14]. A more likely explanation is that Fe has lower site activity (for FT) than Co, but higher WGS activity (in the form of Fe_3O_4), and is more negatively affected by a high water pressure or by low syngas pressures. Hence, the higher Fe-containing catalysts give lower FT productivity but may achieve higher absolute space–time yields of CO_2 (Fig. 9), especially with external water addition. It should be remembered though that even if the nature of the active sites probably is different for WGS and FT, the two reactions are

still competing for the same atoms (but in different oxidation states), which inevitably also will affect the relative extent of the FT and WGS reactions. It should be mentioned that the increased FT activity of the bimetallic catalysts (b) and (c), as compared with the 100% Co catalyst (a), at low conversion (see Section 3.2.1.2) is however not due to the lower relative WGS activities of these, as their absolute WGS activities are actually higher compared with that of catalyst (a) (see "Space-time yield of CO_2" in Table 5).

3.2.3.3. Permanent and reversible deactivation. The catalysts reduce their FT activity (space–time yields of hydrocarbons) of period 2 to 60% (a), 71% (b), 72% (c) and 86% (d) in period 5, respectively. Obviously, the higher the Fe content in these catalysts, the smaller is the apparent permanent deactivation. It should be noted that, generally, Fe-based FT catalysts are reported to have much shorter lifetimes than Co-based. Al_2O_3 has, however, been reported to act as a structural promoter enforcing the formation of spinels at the interface of the Al_2O_3 and a CoFe alloy, thus stabilizing the alloy particles [57].

For catalysts (a–c), the most probable reason for deactivation is sintering accompanied by oxidation. For catalyst (d), however, it is possible that sintering is much less pronounced. One indication of the absence of sintering is the rapid regeneration of the WGS activity upon removal of water from the feed (period $4 \rightarrow 5$). The severe temporary deactivation of catalyst (d) in period 4 with respect to both FT and WGS activity should hence be due to oxidation. For the catalysts (a–d) it thus seems as if the higher Fe-content on the surface, the more severe is the oxidation under conditions with high water partial pressure, while the higher the Fe-content in the bulk of the catalyst the lower is the permanent deactivation.

From the relatively short time-on-stream in the current study, it is not possible to figure out whether the presence of Fe in the Co catalyst reduces the permanent deactivation rate, or if the observed low extent of permanent deactivation for the Fe-containing catalysts is a result of a concurrent deactivation and activation/reconstruction of the iron-rich phases [46,58]. Yet another explanation could be that cobalt migrates towards the surface upon water exposure, resulting in a surface richer in metallic Co, some hours after shutting off the water. The higher FT activity of catalyst (d) compared to the 100% Co catalyst (a) in period 5 (see Table 5) suggests that the iron-rich surface layer of catalyst (d) protects the underlaying cobalt phases (metallic and unreduced) from sintering during water exposure. An indication of an increased surface concentration of cobalt in catalysts (b) and (d) after water exposure is the relatively unchanged selectivity to C_{5+} between period 2 and 5 (see Table 5) despite the decreased conversion. For catalysts (a) and (c), the drop in C_{5+} selectivity from period 2 to 5 is significant, which is expected from a relatively invariant surface when the conversion is decreased. Since catalyst (c) still shows a lower permanent deactivation than (a) it is probable that also the presence of Fe itself prevents sintering.

3.2.4. The WGS equilibrium and kinetics

The space–time yield of hydrocarbons over catalyst 0Fe-100Co (a) for stoichiometric feed ($H_2/CO = 2.1$) has been reported to amount to 0.37 g hydrocarbons (HCs)/g_{cat}.h [59]. No catalyst in the present study (with $H_2/CO = 1.0$) comes close to this value because of poor WGS activities not being able to sustain the H_2/CO ratio throughout the reactor.

Although reaching WGS equilibrium would mean too much shifting for an inlet H_2/CO ratio of 1.0, in all FT experiments presented here the WGS reaction quotient in the gas exiting the reactor has a very low value ($\sim 10^{-3}$–10^{-1}) compared to the equilibrium constant ($\sim$182 at 483 K [60]). In the commercial LTFT synthesis with Fe-based catalysts the WGS equilibrium is not reached because of the low temperature making the WGS reaction slow [5]. In order to improve the WGS activity, a higher temperature and promotion of Fe with alkali are required [9,61]. It has been reported [39] that the relative WGS activity was tripled for a 5 wt% Fe/5 wt% Co/TiO_2 catalyst upon 0.5 wt% K promotion. However, K is a poison to Co, lowering the total activity [39]. Luo et al. [58] have shown promising results for a precipitated iron catalyst promoted with K. They attained usage ratios equal to the molar inlet ratio of $H_2/CO = 0.7$ at 503 K at a syngas conversion of about 40% in a slurry reactor.

3.3. Further work

The development of a Co-based FT catalyst for the direct conversion of H_2-poor biosyngas would be favorable compared to a Fe-based one in that a higher conversion per pass would be possible. Further work should include development of a catalyst in which Co provides most of the FT activity and Fe, or some other compound, essentially provides only WGS activity. A slightly higher reaction temperature and promotion of Fe by alkali would definitely be beneficial for the WGS activity. However, preliminary results from our laboratory have shown that Co is poisoned in the presence of both K and Na, which makes Fe as WGS-active component unsuitable. One possibility would be to use a mechanical mixture of a Cu-based WGS catalyst and a Co catalyst.

4. Conclusion

FTS at 20 bar and 483 K with H_2-poor syngas (H_2/CO ratio = 1.0) was performed over Al_2O_3-supported catalysts with various ratios of Fe:Co (12 wt% bimetal). For bimetallic catalysts prepared by co-impregnation of the metal nitrates, Co was incorporated into the Fe_2O_3 phase, at least for iron-rich samples, while no evidence of Fe incorporated into Co_3O_4 were found. Most probably, iron-rich FeCo alloys were formed upon reduction of these mixed cobalt-iron oxide phases. Cobalt improved the reducibility of iron by preventing the formation of a hard-to-reduce Fe-Al spinel during reduction. Small amounts of Fe might enhance the reducibility of Co, while a pronounced iron surface enrichment at certain Fe:Co ratios seemed to lower the reducibility of Co.

Alloying Co with small/moderate amounts of Fe improved the FT activity of the Co catalyst at low conversion levels. This was accomplished without an increased relative WGS activity, and is therefore thought to be due to a higher FT activity of the Fe-Co mixtures as compared to the pure Co catalyst. Due to unsuccessful chemisorption measurements, it is not possible to decide whether this activity increase should be ascribed to an increased number of active sites, or to an increased TOF. Alloying Fe with small/moderate amounts of Co increased the dispersion of Fe, increased the relative WGS activity and lowered the FT activity of the Fe catalyst, probably due to the FeCo alloy hindering the iron carbide formation and hence resulting in a decreased FT TOF. In general, a higher Fe:Co ratio in the bimetallic catalyst resulted in higher relative WGS activity. However, all catalysts had very low WGS activity, which resulted in low FT productivities (per gram catalyst). Even with external water addition, the WGS activities were poor. The FT activity of a catalyst with relatively high WGS selectivity (i.e. high iron content) was inherently more inhibited by the partial pressure of water (or more sensitive to a reduction in syngas partial pressure), causing a decrease in productivity for the catalysts with the highest relative WGS activity. The catalyst with the highest CO_2 activity was also rapidly deactivated (both as to FT and WGS activities) at high water partial pressures.

From the deactivation profiles it is suggested that for the bimetallic catalysts investigated for five days on stream, i.e. catalysts (a–d), the FT and WGS reactions took place over sites of different nature. The results also indicate that the bimetallic

catalysts (b–d) were more stable against permanent deactivation compared to the pure Co catalyst (a). Still, this would present no advantage during real FT conditions since the bimetallic catalysts suffer from a severe temporary deactivation with respect to both WGS and FT activity upon exposure to the water pressures prevailing at sufficiently high conversion levels. Longer time-on-stream is necessary for determining the true reason for the lower permanent deactivation of the bimetallic catalysts, as compared to the pure Co catalyst.

The bimetallic catalysts showed essentially no synergy effects with respect to HC selectivities and olefin/paraffin ratios. The selectivity values all fell in between those of the single-metal catalysts, which may partly be explained by the use of a sub-stoichiometric inlet H_2/CO ratio. It is striking how the presence of small amounts of Fe affected the C_{5+} selectivity in a negative way, although slightly improving the FT activity.

Fe was enriched at the catalyst surface, at least for the Co-rich samples, covering the Co sites. To achieve high conversion of a H_2-poor syngas, both high WGS and high FT activities are necessary, which is not possible with co-impregnated mixtures of Fe and Co, as it reduces the activity of the significantly more expensive and active Co at high conversions (high partial pressure of water), at least at an iron content high enough for WGS to take place to any significant extent. Both surface enrichment of Fe and iron-rich FeCo alloy formation give the bimetallic catalyst properties closely resembling those of an iron catalyst. For a syngas with a stoichiometric H_2/CO ratio of 2.1, however, the alloying of small amounts of Fe with the Co catalyst might be positive in that the FT activity could be increased.

Acknowledgment

This work was supported by the Swedish Energy Agency. Odd Asbjørn Lindvåg and Rune Myrstad, SINTEF Materials and Chemistry, are acknowledged for help during the experimental part of the work. Magnus Rønning, Department of Chemical Engineering, NTNU, Trondheim, is acknowledged for fruitful discussions.

References

[1] N. Berglin, T. Berntsson, Appl. Therm. Eng. 18 (1998) 94.
[2] M. Johansson, Catalytic combustion of gasified biomass for gas turbine applications, PhD Thesis, Royal Institute of Technology, Stockholm, 1998.
[3] M.E. Dry, Catal. Today 71 (2002) 227.
[4] I. Wender, Fuel Process. Technol. 48 (1996) 189.
[5] M.E. Dry, Appl. Catal. A 138 (1996) 319.
[6] F.G. Botes, B.B. Breman, Ind. Eng. Chem. Res. 45 (2006) 7415.
[7] I.C. Yates, C.N. Satterfield, Energy Fuels 5 (1991) 168.
[8] S. Ledakowicz, H. Nettelhoff, R. Kokuun, W.D. Deckwer, Ind. Eng. Chem. Proc. Des. Dev. 24 (1985) 1043.
[9] H. Schulz, Appl. Catal. A 186 (1999) 3.
[10] A. Raje, J.R. Inga, B.H. Davis, Fuel 76 (1997) 273.
[11] D.J. Duvenhage, N.J. Coville, Appl. Catal. A 153 (1997) 43.
[12] A.A. Mirzaei, R. Habibpour, E. Kashi, Appl. Catal. A 296 (2005) 222.
[13] A.A. Mirzaei, R. Habibpour, M. Faizi, E. Kashi, Appl. Catal. A 301 (2005) 272.
[14] D.J. Duvenhage, N.J. Coville, Appl. Catal. A 289 (2005) 231.
[15] T. Ishihara, K. Eguchi, H. Arai, Appl. Catal. 30 (1987) 225.
[16] J.A. Amelse, L.H. Schwartz, J.B. Butt, J. Catal. 72 (1981) 95.
[17] H. Arai, K. Mitsuishi, T. Seiyama, Chem. Lett. (1984) 1291.
[18] F. Tihay, A.C. Roger, G. Pourroy, A. Kiennemann, Energy Fuels 16 (2002) 1271.
[19] J.L. Lemaitre, P. Govind Menon, F. Delannay, in: F. Delannay (Ed.), Characterization of Heterogeneous Catalysts, vol. 15, Marcel Dekker, New York, 1984, p. 299.
[20] S. Storsæter, Ø. Borg, E.A. Blekkan, A. Holmen, J. Catal. 231 (2005) 405.
[21] J. van de Loosdrecht, E.A. Barradas, E.A. Caricato, N.G. Ngwenya, P.S. Nkwanyana, M.A.S. Rawat, B.H. Sigwebela, P.J. van Berge, J.L. Visagie, Top. Catal. 26 (2003) 121.
[22] Ø. Borg, M. Rønning, S. Storsæter, W. van Beek, A. Holmen, Stud. Surf. Sci. Catal. 163 (2007) 255.
[23] L. Guczi, Catal. Rev. Sci. Eng. 23 (1981) 329.
[24] D. Schanke, Hydrogenation of CO over supported iron catalysts, PhD Thesis, The Laboratory of Industrial Chemistry, The University of Trondheim, The Norwegian Institute of Technology, Trondheim, 1986.
[25] S. Hagen, R. Barfod, R. Fehrmann, C.J.H. Jacobsen, H.T. Teunissen, I. Chorkendorff, J. Catal. 214 (2003) 327.
[26] G. Jacobs, T.K. Das, Y. Zhang, J. Li, G. Racoillet, B.H. Davis, Appl. Catal. A 233 (2002) 263.
[27] A. Moen, D.G. Nicholson, M. Rønning, H. Emerich, J. Mater. Chem. 8 (1998) 2533.
[28] W.K. Jozwiak, E. Kaczmarek, T.P. Maniecki, W. Ignaczak, W. Maniukiewicz, Appl. Catal. A 326 (2007) 17.
[29] R. Brown, M.E. Cooper, D.A. Whan, Appl. Catal. 3 (1982) 177.
[30] J.H.A. Martens, H.F.J. van't Blik, R. Prins, J. Catal. 97 (1986) 200.
[31] E. Manova, T. Tsoncheva, Cl. Estournès, D. Paneva, K. Tenchev, I. Mitov, L. Petrov, Appl. Catal. A 300 (2006) 170.
[32] M.J. Tricker, P.P. Vaishnava, D.A. Whan, Appl. Catal. 3 (1982) 283.
[33] A. Walsh, S.-H. Wei, Y. Yan, M.M. Al-Jassim, J.A. Turner, M. Woodhouse, B.A. Parkinson, Phys. Rev. B 76 (2007) 165119.
[34] M. del Arco, R. Trujillano, V. Rives, J. Mater. Chem. 8 (1998) 761.
[35] E. van Steen, M. Claeys, M.E. Dry, J. van de Loosdrecht, E.L. Viljoen, J.L. Visagie, J. Phys. Chem. B 109 (2005) 3575.
[36] F. Huber, Z. Yu, S. Lögdberg, M. Rønning, D. Chen, H. Venvik, A. Holmen, Catal. Lett. 110 (2006) 211.
[37] Q. Hao, L. Bai, Y. Li, X. Li, H. Xiang, Y. Li, Cuihua Xuebao 26 (2005) 791.
[38] G. van der Laan, A. Beenackers, Ind. Eng. Chem. Res. 38 (1999) 1277.
[39] D.J. Duvenhage, N.J. Coville, Catal. Lett. 104 (2005) 129.
[40] H.-J. Wan, B.-S. Wu, C.-H. Zhang, B.-T. Teng, Z.-C. Tao, Y. Yang, Y.-L. Zhu, H.-W. Xiang, Y.-W. Li, Fuel 85 (2006) 1371.
[41] A.P. Raje, R.J. O'Brien, B.H. Davis, J. Catal. 180 (1998) 36.
[42] S. Li, S. Krishnamoorthy, A. Li, G.D. Meitzner, E. Iglesia, J. Catal. 206 (2002) 202.
[43] C.N. Satterfield, R.T. Hanlon, S.E. Tung, Z. Zou, G.C. Papaefthymiou, Ind. Eng. Chem. Prod. Res. Dev. 25 (1986) 401.
[44] S. Li, R.J. O?Brien, G.D. Meitzner, H. Hamdeh, B.H. Davis, E. Iglesia, Appl. Catal. A 219 (2001) 215.
[45] C.S. Kuivila, P.C. Stair, J.B. Butt, J. Catal. 118 (1989) 299.
[46] T. Herranz, S. Rojas, F.J. Pérez-Alonso, M. Ojeda, P. Terrero, J.L.G. Fierro, Appl. Catal. A 308 (2006) 19.
[47] J.F. Bengoa, A.M. Alvarez, M.V. Cagnoli, N.G. Gallegos, S.G. Marchetti, Appl. Catal. A 325 (2007) 68.
[48] B.T. Teng, J. Chang, J. Yang, G. Wang, C.H. Zhang, Y.Y. Xu, H.W. Xiang, Y.W. Li, Fuel 84 (2005) 917.
[49] E. Iglesia, Appl. Catal. A 161 (1997) 59.
[50] D.J. Duvenhage, N.J. Coville, Appl. Catal. A 298 (2006) 211.
[51] D.S. Newsome, Catal. Rev. Sci. Eng. 21 (1980) 27.
[52] J. van de Loosdrecht, B. Balzhinimaev, J.-A. Dalmon, J.W. Niemantsverdriet, S.V. Tsybulya, A.M. Saib, P.J. van Berge, J.L. Visagie, Catal. Today 123 (2007) 293.
[53] F.M. Gottschalk, G.J. Hutchings, Appl. Catal. 51 (1989) 127.
[54] Y.N. Wang, W.P. Ma, Y.J. Lu, J. Yang, Y.Y. Xu, H.W. Xiang, Y.W. Li, Y.L. Zhao, B.J. Zhang, Fuel 82 (2003) 195.
[55] C.N. Satterfield, R.T. Hanlon, S.E. Tung, Z. Zou, G.C. Papaefthymiou, Ind. Eng. Chem. Prod. Res. Dev. 25 (1986) 407.
[56] W. Ning, N. Koizumi, H. Chang, T. Mochizuki, T. Itoh, M. Yamada, Appl. Catal. A 312 (2006) 35.
[57] T.V. Reshetenko, L.B. Avdeeva, A.A. Khassin, G.N. Kustova, V.A. Ushakov, E.M. Moroz, A.N. Shmakov, V.V. Kriventsov, D.I. Kochubey, Y.T. Pavlyukhin, A.L. Chuvilin, Z.R. Ismagilov, Appl. Catal. A 268 (2004) 127.
[58] M. Luo, R.J. O'Brian, S. Bao, B.H. Davis, Appl. Catal. A 239 (2003) 111.
[59] D. Tristantini, S. Lögdberg, B. Gevert, Ø. Borg, A. Holmen, Fuel Process. Technol. 88 (2007) 643.
[60] H. Purnama, T. Ressler, R.E. Jentoft, H. Soerijanto, R. Schlögl, R. Schomäcker, Appl. Catal. A 259 (2004) 83.
[61] A. Holmen, D. Schanke, G. Sundmark, Appl. Catal. 50 (1989) 211.